Computational Mechanics (2022) 69:805–824
https://doi.org/10.1007/s00466-021-02115-0

ORIGINAL PAPER

An electromechanically coupled beam model for dielectric elastomer actuators

Dengpeng Huang[1] · **Sigrid Leyendecker**[1]

Received: 12 July 2021 / Accepted: 31 October 2021 / Published online: 25 November 2021

Abstract
In this work, the Cosserat formulation of geometrically exact beam dynamics is extended by adding the electric potential as an additional degree of freedom to account for the electromechanical coupling in the dielectric elastomer actuators. To be able to generate complex beam deformations via dielectric actuator, a linear distribution of electric potential on the beam cross section is proposed. Based on this electric potential, the electric field and the strain-like electrical variable are defined for the beam, where the strain-like electrical variable is work-conjugated to the electric displacement. The electromechanically coupled strain energy for the beam is derived consistently from continuum electromechanics, which leads to the direct application of the material models in the continuum to the beam model. The electromechanically coupled problem in beam dynamics is first spatially semidiscretized by 1D finite elements and then solved via variational time integration. By applying different electrical boundary conditions, different deformations of the beam are obtained in the numerical examples, including contraction, shear, bending and torsion. The damping effect induced by the viscosity as well as the total energy of the beam are evaluated. The deformations of the electromechanically coupled beam model are compared with the results of the 3D finite element model, where a good agreement of the deformations in the beam model and that in the 3D finite element model is observed. However, less degrees of freedom are required to resolve the complex deformations in the beam model.

Keywords Dielectric elastomer actuators · Variational integrator · Electromechanical coupling · Geometrically exact beam

1 Introduction

With the wide application of robotics in industrial production, medical treatment and daily life, better performances of robotic systems are demanded, such as a higher efficiency in energy, completing complex tasks and a safe interaction with environment. To cope with these challenges, the dielectric elastomer actuators (DEAs) have been developed to serve as artificial muscles for soft robotics, see e.g. [5,9,14,17]. The DEA is essentially composed by multiple stacked capacitors where the dielectric elastomer is sandwiched between two compliant electrodes. When an external electric field is applied to the DEA, the dielectric material will be polarized, resulting in electrostatic pressure, see the models in [21,25,31,34] for instance. Due to the contractive pressure, the contraction of the DEA will be induced such that it can be applied as an actuator. The deformation behavior of the DEA is governed by the electromechanical coupling in the dielectric material.

For the general investigation of the electromechanical coupling behavior, much effort has been made to address the nonlinear electroelasticity in the past years, see e.g. the theory of interaction of electromagnetic and elastic fields in deformable continua in [20], the nonlinear electroelasticity formulation for the finite deformation in [8] and the variational formulations of the electro- and magneto-elastostatics in [33]. Additionally, material models of the dielectric elastomers have been investigated, see e.g. [30,33,36]. The instabilities of dielectric membranes are investigated in [12]. In [13], a viscoelastic effect is introduced to account for the damped dynamic behavior in silicon based dielectric elastomers. A viscoelastic 3D finite element model of the DEA is developed by [24] for the dynamic analysis using a structure preserving time integration scheme. This model is extended to flexible multibody system dynamics in [23].

✉ Dengpeng Huang
dengpeng.huang@fau.de

[1] Institute of Applied Dynamics,
Friedrich-Alexander-Universität Erlangen-Nürnberg,
Immerwahrstrasse 1, D-91058 Erlangen, Germany

The finite element models introduced above provide a powerful and accurate tool for solving the electromechanical coupling problem in DEA. However, huge amounts of degrees of freedom are required in large 3D finite element models, which leads to inefficient computation and difficulties for the optimal control of DEA. Especially for long thin artificial muscles, 3D finite element model is more expensive in computational cost than beam model. Further more, the coupling between 3D finite element models and rigid body is possible but has to be specially addressed in multibody system. The geometrically exact beam performs well concerning the tradeoff between computational cost and accuracy for the simulation of slender structures like the stacked DEA. By assigning the rotational degrees of freedom to points in continuum, the Cosserat formulation [7] of geometrically exact beam closes the gap between classical continuum mechanics and rigid (multi-)body dynamics, which leads to a consistent formulation of flexible multibody systems. The fundamental formulations on geometrically exact beam can be found in [2,27] for instance. The time integration of constrained geometrically nonlinear beam dynamics has been discussed by many authors, see e.g. the energy conserving/decaying algorithms in [3], the energy–momentum scheme with null space method in [6] and the variational integrators in [16]. An energy–momentum integrator is applied in the nonlinear electro-elastodynamics by [19]. To account for the electric field in a beam, the focus has been put on the piezoelectric effect, see [15,26,32]. An analytical model for dielectric elastomer based microbeam is discussed in [11]. However, the electromechanically coupled problem of dielectric elastomers in geometrically exact beam is still not given.

The objective of this work is to develop an electromechanically coupled beam model for the simulation of stacked dielectric elastomer actuators, where the Cosserat formulation of geometrically exact beam dynamics is extended by adding the electric potential as the additional degree of freedom. A linear distribution of electric potential on the beam cross section is proposed to generate different beam deformations including contraction, shear, bending and torsion. The electric field in the beam is computed from the gradient of the electric potential. Based on the formulation of deformation gradient and electric field in the beam, the electromechanically coupled strain energy function for the beam is derived consistently from the strain energy function in continuum electromechanics, which leads to the direct application of the material models in continuum electromechanics to the beam model. The viscoelastic effect is taken into account in the non-conservative force term. The electromechanically coupled problem in beam dynamics is first semidiscretized with 1D spatial finite elements and then solved via variational time integration. By applying different electrical boundary conditions, different deformations of the beam are obtained in the numerical examples, which are compared with the results of the 3D finite element model.

This paper is structured as follows: In Sects. 2 and 3, the governing equations for electromechanical coupling in continuum electromechanics and geometrically exact beam are presented, respectively. Then the formulation of kinematic variables including the deformation gradient, the electric potential and the electric field are derived for the beam in Sect. 4. Section 5 presents the consistent derivation of a strain energy function for the beam from continuum electromechanics. In Sect. 6, the electromechanical coupling problem is solved within the variational time integration scheme with null space projection. The numerical examples of the developed model are presented in Sect. 7, followed by the conclusions in Sect. 8.

2 Governing equations for electromechanical coupling in continuum electromechanics

The finite deformation of a dielectric elastic solid occupying the domain $B \subset \mathbb{R}^3$ is distinguished by the initial and current configurations. The boundary of the solid ∂B is composed by the Dirichlet type sections $\partial_u B$ and $\partial_\phi B$, and the Neumann type sections $\partial_\sigma B$ and $\partial_D B$. By denoting the position of a material point in the initial configuration with $\mathbf{X} \in B_0$, the position of the material point in the current configuration at time t is given by

$$\mathbf{x} = \mathbf{X} + \mathbf{u}(\mathbf{X}, t), \tag{1}$$

where $\mathbf{u}$ is the displacement. The deformations within the body induced by the electric field satisfy the balance law of momentum and the Maxwell equations.

2.1 Balance of linear and angular momentum

The local balance law of linear momentum in the dynamic process is given by

$$\nabla_{\mathbf{X}} \cdot \mathbf{P} + \rho_0 \bar{\mathbf{b}} = \rho_0 \ddot{\mathbf{u}} \quad \text{in} \quad B, \tag{2}$$

subject to the Dirichlet and Neumann boundary conditions

$$\mathbf{u} = \bar{\mathbf{u}} \quad \text{on} \quad \partial_u B, \tag{3}$$

$$\mathbf{P} \cdot \mathbf{N} = \bar{\mathbf{T}} \quad \text{on} \quad \partial_\sigma B, \tag{4}$$

where $\mathbf{P}$ is the first Piola–Kirchhoff stress tensor, ρ_0 is the mass density in initial configuration, $\bar{\mathbf{b}}$ is the body force vector, $\ddot{\mathbf{u}}$ is the acceleration, $\bar{\mathbf{u}}$ is the prescribed displacement and $\bar{\mathbf{T}}$ is the prescribed traction. The local balance of angular momentum reads

$$\mathbf{F}\mathbf{P}^T = \mathbf{P}\mathbf{F}^T, \tag{5}$$

in which $\mathbf{F}$ is the deformation gradient defined as $\mathbf{F} = \partial\mathbf{x}(\mathbf{X}, t)/\partial\mathbf{X}$.

2.2 Maxwell equations

By neglecting the magnetic field, the Maxwell equations are given by

$$\nabla_{\mathbf{X}} \times \mathbf{E}^e = \mathbf{0}, \quad \nabla_{\mathbf{X}} \cdot \mathbf{D} = 0 \quad \text{in} \quad B, \tag{6}$$

subject to the Dirichlet and Neumann boundary conditions

$$\phi = \bar{\phi} \quad \text{on} \quad \partial_\phi B, \tag{7}$$

$$\mathbf{D} \cdot \mathbf{N} = \bar{Q} \quad \text{on} \quad \partial_D B, \tag{8}$$

with $\mathbf{E}^e$ the electric field, $\mathbf{D}$ the electric displacement in the initial configuration, ϕ the electric potential, $\bar{\phi}$ the prescribed electric potential, $\mathbf{N}$ the outward unit normal vector and $\bar{Q}$ the prescribed charges per unit area on the boundary $\partial_D B$. The Eq. $(6)_1$ leads to the definition of the electric field as the gradient of a scalar electric potential

$$\mathbf{E}^e = -\frac{\partial \phi}{\partial \mathbf{X}}. \tag{9}$$

2.3 Electromechanical coupling

When the external electric field is imposed in the body of dielectric elastomer, the contractive pressure will be induced due to the polarization effects and thus the deformation of the body will be generated. The coupling effect between the electric field and the mechanical deformation is described by the strain energy function $\Omega(\mathbf{F}, \mathbf{E}^e)$ of the dielectric material in the constitutive equations

$$\mathbf{D} = -\rho_0 \frac{\partial \Omega(\mathbf{F}, \mathbf{E}^e)}{\partial \mathbf{E}^e}, \quad \mathbf{P} = \rho_0 \frac{\partial \Omega(\mathbf{F}, \mathbf{E}^e)}{\partial \mathbf{F}}. \tag{10}$$

For the dielectric materials, the electromechanical coupling can be described by the strain energy function with the additive form

$$\Omega(\mathbf{F}, \mathbf{E}^e) = \Omega^m(\mathbf{F}) + \Omega^{\mathrm{em}}(\mathbf{F}, \mathbf{E}^e) + \Omega^e(\mathbf{E}^e), \tag{11}$$

with $\Omega^m(\mathbf{F})$ referring to the purely mechanical behavior, $\Omega^{\mathrm{em}}(\mathbf{F}, \mathbf{E}^e)$ referring to the electomechanical coupling and $\Omega^e(\mathbf{E}^e)$ referring to the pure electric behavior. Accordingly, the first Piola–Kirchhoff stress can be written as two parts

$$\mathbf{P} = \rho_0 \frac{\partial \Omega^m}{\partial \mathbf{F}} + \rho_0 \frac{\partial \Omega^{em}}{\partial \mathbf{F}}. \tag{12}$$

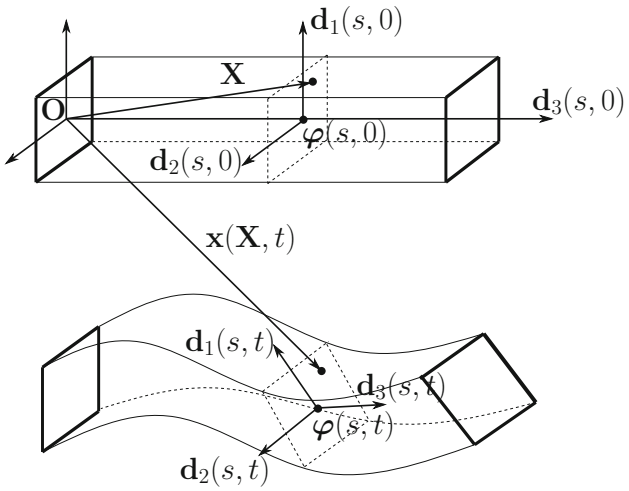

Fig. 1 Configurations of the beam

3 Governing equations for electromechanical coupling in geometrically exact beam

In this work, the formulation of the electromechanical coupling problem presented above is extended to the geometrically exact beam. The deformation state of an initially straight beam over time can be distinguished by the initial configuration and the current configuration, as shown in Fig. 1.

In the Cosserat formulation of geometrically exact beam, the placement of a material point in the current configuration of the beam is given by

$$\mathbf{x}(X^k, s, t) = \boldsymbol{\varphi}(s, t) + X^k \mathbf{d}_k(s, t), \quad k = 1, 2. \tag{13}$$

where $s \in [0, L] \subset \mathbb{R}$ denotes the arc-length of the line of the centroids $\boldsymbol{\varphi}(s, 0) \in \mathbb{R}^3$ in the initial configuration, $\mathbf{d}_i(s, t)$ is an orthonormal triad at s with the directors $\mathbf{d}_k(s, t)$, $k = 1, 2$ spanning a principle basis of the cross section, and X^k are the curvilinear coordinates on the cross section. Based on these assumptions, the governing equations for electromechanically coupled beam model can be consistently derived from the equations of continuum electromechanics.

3.1 Electromechanically coupled beam model in variational setting

The governing equations of the beam are usually derived by integrating Eq. (2) in continuum mechanics over the beam cross section, see e.g. [27]. However, the internal lateral traction on the contour of beam cross section appearing during the integration of the divergence term and the external lateral traction (as Neumann boundary condition) are not clearly distinguished. To obtain a consistent derivation of

beam equations from continuum mechanics considering the Neumann boundary conditions in Eqs. (4) and (8), in this work, we formulate the governing equations for the beam from the variational setting.

The variational setting is formulated according to the Lagrange–d'Alembert principle

$$\delta S + \int_0^T \delta W^{\text{ext}} dt = 0, \tag{14}$$

with the action S defined as the space-time integral $S = \int_0^T \int_{B_0} L dV dt$ over the Lagrange density L and W^{ext} the external non-conservative work contributed by the body force and surface traction. According to the constitutive law in Eq. (10), the variation of the action can be formulated for the beam as

$$\begin{aligned}\delta S &= \int_0^T \int_{B_0} \left(\rho_0 \dot{\mathbf{x}} \cdot \delta \dot{\mathbf{x}} - \partial_{\mathbf{F}} \Omega : \delta \mathbf{F} - \partial_{\mathbf{E}^e} \Omega \cdot \delta \mathbf{E}^e\right) dV dt \\ &= \int_0^T \left\{ \int_c \int_\Sigma \left[\delta \mathbf{x} \cdot \left(-\rho_0 \ddot{\mathbf{x}} + \nabla_{\mathbf{X}} \cdot \mathbf{P}\right) + \delta\phi \left(-\nabla_{\mathbf{X}} \cdot \mathbf{D}\right)\right] dA ds \right. \\ &\quad \left. + \int_c \oint_{\partial\Sigma} \left[\delta \mathbf{x} \cdot \left(-\mathbf{P} \cdot \mathbf{N}\right) + \delta\phi \left(\mathbf{D} \cdot \mathbf{N}\right)\right] dl ds \right\} dt, \end{aligned} \tag{15}$$

where the formula $-\partial_{\mathbf{F}} \Omega : \delta \mathbf{F} = (\nabla_{\mathbf{X}} \cdot \partial_{\mathbf{F}} \Omega) \cdot \delta \mathbf{x} - \nabla_{\mathbf{X}} \cdot (\partial_{\mathbf{F}} \Omega \cdot \delta \mathbf{x})$ and the divergence theorem have been applied. In the derivation of Eq. (15), the end-point conditions in time, i.e. $\delta \mathbf{x}_0 = \delta \mathbf{x}_T = \mathbf{0}$, have been applied. Due to the assumption of geometrically exact beam, the volume integral in Eq. (15) is split into the curve integral over beam center line and the area integral over beam cross section Σ. At the same time, the surface integral in Eq. (15) is split into the curve integral over beam center line and the curve integral over the lateral contour of beam cross section. By using of $\mathbf{P} = \mathbf{t}_k \otimes \mathbf{d}_k(s,0) + \mathbf{t}_s \otimes \mathbf{d}_3(s,0)$ and $\mathbf{D} = D_i \mathbf{d}_i(s,0) (i = 1,2,3)$, the force $\mathbf{f}$, the torque $\mathbf{m}$ and the electric displacement d_s^e for the beam are defined as

$$\mathbf{f} = \int_\Sigma \mathbf{t}_s dA, \qquad \mathbf{m} = \int_\Sigma \mathbf{r} \times \mathbf{t}_s dA, \qquad d_s^e = \int_\Sigma D_3 dA, \tag{16}$$

with $\mathbf{r} = \mathbf{x} - \boldsymbol{\varphi}$. For the sake of later use, the electric displacement vector $\mathbf{d}^e$ for the beam is defined as $\mathbf{d}^e = \left[d_1^e \; d_2^e \; d_s^e\right]^T$ with the components $d_k^e = \int_\Sigma D_k dA$. In this case, the divergence terms in Eq. (15) can be formulated as

$$\int_\Sigma \nabla_{\mathbf{X}} \cdot \mathbf{P} dA = \underbrace{\int_\Sigma \frac{\partial \mathbf{t}_1}{\partial X_1} + \frac{\partial \mathbf{t}_2}{\partial X_2} dA}_{\mathbf{f}^n} + \frac{\partial \mathbf{f}}{\partial s}, \tag{17}$$

$$\int_\Sigma \mathbf{r} \times \nabla_{\mathbf{X}} \cdot \mathbf{P} dA = \underbrace{\int_\Sigma \mathbf{r} \times \left(\frac{\partial \mathbf{t}_1}{\partial X_1} + \frac{\partial \mathbf{t}_2}{\partial X_2}\right) dA}_{\mathbf{m}^n} + \frac{\partial \mathbf{m}}{\partial s} + \frac{\partial \boldsymbol{\varphi}}{\partial s} \times \mathbf{f}, \tag{18}$$

$$\int_\Sigma \nabla \cdot \mathbf{D} dA = \underbrace{\int_\Sigma \frac{\partial D_1}{\partial X_1} + \frac{\partial D_2}{\partial X_2} dA}_{d^{en}} + \frac{\partial d_s^e}{\partial s}. \tag{19}$$

In the surface integral of Eq. (15), the unit normal vector is in the plane of cross section, i.e. $\mathbf{N} = n_k \mathbf{d}_k(s,0) (k = 1,2)$. Thus, by applying the divergence theorem, we have $\oint_{\partial\Sigma} \mathbf{P} \cdot \mathbf{N} dl = \mathbf{f}^n$, $\oint_{\partial\Sigma} \mathbf{r} \times (\mathbf{P} \cdot \mathbf{N}) dl = \mathbf{m}^n$ and $\oint_{\partial\Sigma} \mathbf{D} \cdot \mathbf{N} dl = d^{en}$. The variation of the position field is given by

$$\delta \mathbf{x} = \delta \boldsymbol{\varphi} + \delta \boldsymbol{\eta} \times \mathbf{r}, \tag{20}$$

with $\delta \boldsymbol{\eta} = \frac{1}{2} \mathbf{d}^i \times \delta \mathbf{d}_i$, see the details in [10]. The time derivatives of the position field are given by

$$\dot{\mathbf{x}} = \dot{\boldsymbol{\varphi}} + \boldsymbol{\omega} \times \mathbf{r}, \qquad \ddot{\mathbf{x}} = \ddot{\boldsymbol{\varphi}} + \dot{\boldsymbol{\omega}} \times \mathbf{r} + \boldsymbol{\omega} \times \boldsymbol{\omega} \times \mathbf{r}, \tag{21}$$

with $\boldsymbol{\omega}$ the spatial angular velocity. Using Eqs. (19)–(21), the varitation of the action in Eq. (15) reads

$$\begin{aligned}\delta S &= \int_c \left[\delta \boldsymbol{\varphi} \cdot \left(-A_\rho \ddot{\boldsymbol{\varphi}} + \mathbf{f}^n + \frac{\partial \mathbf{f}}{\partial s}\right) \right. \\ &\quad + \delta \boldsymbol{\eta} \cdot \left(-\dot{\boldsymbol{\omega}} \mathbb{I} - \boldsymbol{\omega} \times \boldsymbol{\omega} \mathbb{I} + \mathbf{m}^n + \frac{\partial \mathbf{m}}{\partial s} + \frac{\partial \boldsymbol{\varphi}}{\partial s} \times \mathbf{f}\right) \\ &\quad \left. + \delta\phi \left(-d^{en} - \frac{\partial d_s^e}{\partial s}\right)\right] ds \\ &\quad + \int_c \left[\delta \boldsymbol{\varphi} \cdot \left(-\mathbf{f}^n\right) + \delta \boldsymbol{\varphi} \cdot \left(-\mathbf{m}^n\right) + \delta\phi \, d^{en}\right] ds, \end{aligned} \tag{22}$$

in which $\mathbb{I} = \int_\Sigma \rho \left(\|\mathbf{x}\|^2 \mathbf{I} - \mathbf{x} \otimes \mathbf{x}\right) dA$ is the spatial mass moment of inertia tensor. It can be observed that $\mathbf{f}^n$ and $\mathbf{m}^n$ in the first curve integral of Eq. (22) come from the divergence term of the action in Eq. (15), $\mathbf{f}^n$ and $\mathbf{m}^n$ in the second curve integral of Eq. (22) come from the integration over a boundary surface in Eq. (15). Due to their opposite signs, they will be offset respectively.

By considering the Neumann boundary conditions in Eqs. (4) and (8), the variation of the external work is written as

$$\begin{aligned}\delta W^{\text{ext}} &= \int_{B_0} \delta \mathbf{x} \cdot \rho_0 \bar{\mathbf{b}} dV + \int_{\partial B_0} \delta \mathbf{x} \cdot \bar{\mathbf{T}} dA \\ &\quad + \int_{\partial B_0} \delta\phi \, \bar{Q} dA \\ &= \int_c \delta \boldsymbol{\varphi} \cdot \bar{\mathbf{f}} ds + \int_c \delta \boldsymbol{\varphi} \cdot \bar{\mathbf{t}} ds + \int_c \delta \boldsymbol{\eta} \cdot \bar{\mathbf{m}} ds \\ &\quad + \int_c \delta \boldsymbol{\eta} \cdot \bar{\boldsymbol{\tau}} ds + \int_c \delta\phi \, \bar{q} ds, \end{aligned} \tag{23}$$

where the prescribed body force, lateral traction, torque and lateral charge are defined respectively as

$$\bar{\mathbf{f}} = \int_\Sigma \rho_0 \bar{\mathbf{b}} dA, \quad \bar{\mathbf{t}} = \oint_{\partial\Sigma} \bar{\mathbf{T}} dl, \quad \bar{\mathbf{m}} = \int_\Sigma \mathbf{r} \times \rho_0 \bar{\mathbf{b}} dA,$$
$$\bar{\boldsymbol{\tau}} = \oint_{\partial\Sigma} \mathbf{r} \times \bar{\mathbf{T}} dl, \quad \bar{q} = \oint_{\partial\Sigma} \bar{Q} dl. \tag{24}$$

Combing Eqs. (22) and (23), the Lagrange–d'Alembert principle for the beam is given by

$$\int_0^T \left\{ \int_c \left[\delta\boldsymbol{\varphi} \cdot \left(-A_\rho \ddot{\boldsymbol{\varphi}} + \frac{\partial \mathbf{f}}{\partial s} + \bar{\mathbf{f}} + \bar{\mathbf{t}} \right) \right.\right.$$
$$+ \delta\boldsymbol{\eta} \cdot \left(-\dot{\boldsymbol{\omega}}\mathbb{I} - \boldsymbol{\omega} \times \boldsymbol{\omega}\mathbb{I} + \frac{\partial \mathbf{m}}{\partial s} + \frac{\partial \boldsymbol{\varphi}}{\partial s} \times \mathbf{f} + \bar{\mathbf{m}} + \bar{\boldsymbol{\tau}} \right)$$
$$\left.\left. + \delta\phi \left(-\frac{\partial d_s^e}{\partial s} + \bar{q} \right) \right] ds \right\} dt = 0 \tag{25}$$

3.2 Balance of linear and angular momentum

The requirement of stationary in Eq. (25) in terms of the translation field $\boldsymbol{\varphi}$ leads to the balance of linear momentum for the beam

$$\frac{\partial \mathbf{f}}{\partial s} + \bar{\mathbf{f}} + \bar{\mathbf{t}} = A_\rho \ddot{\boldsymbol{\varphi}} \qquad s \in [0, L]. \tag{26}$$

The requirement of stationary in Eq. (25) in terms of the rotation field $\boldsymbol{\eta}$ leads to the balance of the angular momentum for the beam

$$\frac{\partial \mathbf{m}}{\partial s} + \frac{\partial \boldsymbol{\varphi}}{\partial s} \times \mathbf{f} + \bar{\mathbf{m}} + \bar{\boldsymbol{\tau}} = \mathbb{I}\dot{\boldsymbol{\omega}} + \boldsymbol{\omega} \times \mathbb{I}\boldsymbol{\omega} \qquad s \in [0, L]. \tag{27}$$

3.3 Maxwell equation

The requirement of stationary in Eq. (25) in terms of the electric potential ϕ leads to the Maxwell equation for the beam

$$\frac{\partial d_s^e}{\partial s} - \bar{q} = 0 \qquad s \in [0, L]. \tag{28}$$

3.4 Electromechanical coupling

The force $\mathbf{f}$, the torque $\mathbf{m}$ and the electric displacement vector $\mathbf{d}^e$ in the beam governing equations are related with the kinematic variables via the constitutive equations

$$\mathbf{d}^e = -\rho_0 \frac{\partial \Omega_b(\boldsymbol{\gamma}, \boldsymbol{\kappa}, \boldsymbol{\varepsilon})}{\partial \boldsymbol{\varepsilon}}, \quad \mathbf{f} = \rho_0 \frac{\partial \Omega_b(\boldsymbol{\gamma}, \boldsymbol{\kappa}, \boldsymbol{\varepsilon})}{\partial \boldsymbol{\gamma}},$$
$$\mathbf{m} = \rho_0 \frac{\partial \Omega_b(\boldsymbol{\gamma}, \boldsymbol{\kappa}, \boldsymbol{\varepsilon})}{\partial \boldsymbol{\kappa}}, \tag{29}$$

where Ω_b is the strain energy per unit arc-length in a beam, $\boldsymbol{\varepsilon}$ is the strain-like electrical variable conjugated with the electric displacement $\mathbf{d}^e$ of the beam, $\boldsymbol{\gamma}$ and $\boldsymbol{\kappa}$ are the beam strain measures conjugated with $\mathbf{f}$ and $\mathbf{m}$, respectively. The electromechanical coupling can be specified by the strain energy function in the additive form

$$\Omega_b(\boldsymbol{\gamma}, \boldsymbol{\kappa}, \boldsymbol{\varepsilon}) = \Omega_b^m(\boldsymbol{\gamma}, \boldsymbol{\kappa}) + \Omega_b^{\mathrm{em}}(\boldsymbol{\gamma}, \boldsymbol{\kappa}, \boldsymbol{\varepsilon}) + \Omega_b^e(\boldsymbol{\varepsilon}). \tag{30}$$

Due to the coupled term in strain energy, the force and torque are contributed by two parts accordingly, the electric part and the mechanical part, i.e.

$$\mathbf{f} = \rho_0 \frac{\partial \Omega_b^m}{\partial \boldsymbol{\gamma}} + \rho_0 \frac{\partial \Omega_b^{em}}{\partial \boldsymbol{\gamma}}, \qquad \mathbf{m} = \rho_0 \frac{\partial \Omega_b^m}{\partial \boldsymbol{\kappa}} + \rho_0 \frac{\partial \Omega_b^{em}}{\partial \boldsymbol{\kappa}}. \tag{31}$$

4 Mechanical and electrical kinematics in the beam

To compute the force $\mathbf{f}$, the torque $\mathbf{m}$ and the electric displacement $\mathbf{d}^e$ in the governing equations of the electromechanically coupled beam model in Sect. 3, the conjugated kinematic variables for mechanical and electrical parts have to be formulated. The mechanical strain measures $\boldsymbol{\gamma}$ and $\boldsymbol{\kappa}$ for the geometrically exact beam have been defined and related with the deformation gradient in the literature, see e.g. [4]. However, the electric potential ϕ as well as the strain-like electrical variable $\boldsymbol{\varepsilon}$ are still not given for the beam.

4.1 Mechanical kinematics in the beam

By setting the origin of the global Cartesian coordinate system $\mathbf{O}$ to one end of the beam as shown in Fig. 1, the location of the node $\boldsymbol{\varphi}(s, 0)$ of the straight beam can be rewritten in terms of the director $\mathbf{d}_3(s, 0)$ and the arc length s

$$\boldsymbol{\varphi}(s, 0) = X^3 \mathbf{d}_3(s, 0) = s\mathbf{d}_3(s, 0), \quad \text{or} \quad X^3 = s. \tag{32}$$

Thus the components X^i of the vector $\mathbf{X}$ in the initial configuration can be computed by projecting the position vector to the directors

$$X^i = \mathbf{X} \cdot \mathbf{d}_i(s, 0), \quad i = 1, 2, 3. \tag{33}$$

By applying Eqs. (13) and (33), the deformation gradient at a point (X^1, X^2, s) in the beam can be written as, see [4],

$$\mathbf{F}(X^1, X^2, s, t) = \frac{\partial \mathbf{x}}{\partial \mathbf{X}} = \frac{\partial \mathbf{x}}{\partial X_i} \otimes \mathbf{d}_i(s,0) = \left[\mathbf{I} + \left(\frac{\partial \boldsymbol{\varphi}(s,t)}{\partial s} - \mathbf{d}_3(s,t) + X^1 \frac{\partial \mathbf{d}_1(s,t)}{\partial s} + X^2 \frac{\partial \mathbf{d}_2(s,t)}{\partial s}\right) \otimes \mathbf{d}_3(s,t)\right] \boldsymbol{\Lambda}(s), \tag{34}$$

with the rotation tensor $\boldsymbol{\Lambda}(s) = \mathbf{d}_i(s,t) \otimes \mathbf{d}_i(s,0)$ and $\boldsymbol{\Lambda}(s)^{-1} = \boldsymbol{\Lambda}(s)^T$. The derivatives in Eq. (34) can be written in terms of the beam strain measures, such as $\frac{\partial \mathbf{d}_k(s,t)}{\partial s}$ is related to the strain $\boldsymbol{\kappa}$ for bending and torsion by

$$\frac{\partial \mathbf{d}_k(s,t)}{\partial s} = \boldsymbol{\kappa}(s,t) \times \mathbf{d}_k(s,t) = \left[\kappa_j \mathbf{d}_j(s,t)\right] \times \mathbf{d}_k(s,t), \tag{35}$$

and $\frac{\partial \boldsymbol{\varphi}(s,t)}{\partial s}$ is related to the strain $\boldsymbol{\gamma}$ for shear and elongation by

$$\frac{\partial \boldsymbol{\varphi}(s,t)}{\partial s} - \mathbf{d}_3(s,t) = \boldsymbol{\gamma}(s,t). \tag{36}$$

Consequently, the deformation gradient $\mathbf{F}$ in Eq. (34) can be further formulated in terms of the beam strain measures as

$$\mathbf{F} = \left\{\mathbf{I} + \left[\boldsymbol{\gamma}(s,t) + \boldsymbol{\kappa}(s,t) \times X^k \mathbf{d}_k(s,t)\right] \otimes \mathbf{d}_3(s,t)\right\} \boldsymbol{\Lambda}(s) = \left[\mathbf{I} + \mathbf{a}(s,t) \otimes \mathbf{d}_3(s,t)\right] \boldsymbol{\Lambda}(s) \tag{37}$$

with $\mathbf{a}(s,t) = \boldsymbol{\gamma}(s,t) + \boldsymbol{\kappa}(s,t) \times X^k \mathbf{d}_k(s,t)$. The variable $\mathbf{a}$ can be formulated in the reference configuration with the beam strain measures $\boldsymbol{\Gamma}$ and $\mathbf{K}$

$$\mathbf{a}^r = \boldsymbol{\Lambda}^T \mathbf{a} = \boldsymbol{\Gamma} + \mathbf{K} \times X^k \mathbf{d}_k^0. \tag{38}$$

The determinant of the deformation gradient reads

$$J = \det(\mathbf{F}) = 1 + \mathbf{a}(s,t) \cdot \mathbf{d}_3(s,t). \tag{39}$$

Accordingly, the Green-Lagrange strain and the right Cauchy Green tensor are given by

$$\mathbf{E} = \left[\mathbf{a}^r \otimes \mathbf{d}_3(s,0)\right]^{\text{sym}} + \frac{1}{2}(\mathbf{a}^r \cdot \mathbf{a}^r)\mathbf{d}_3(s,0) \otimes \mathbf{d}_3(s,0), \tag{40}$$

$$\mathbf{C} = \mathbf{I} + 2\left[\mathbf{a}^r \otimes \mathbf{d}_3(s,0)\right]^{\text{sym}} + (\mathbf{a}^r \cdot \mathbf{a}^r)\mathbf{d}_3(s,0) \otimes \mathbf{d}_3(s,0). \tag{41}$$

The inverse of the right Cauchy Green tensor can be formulated as

$$\mathbf{C}^{-1} = \mathbf{F}^{-1}\mathbf{F}^{-T} = \boldsymbol{\Lambda}^{-1}\mathbf{A}^{-1}\mathbf{A}^{-T}\boldsymbol{\Lambda}^{-T} = \boldsymbol{\Lambda}^T\mathbf{A}^{-1}\mathbf{A}^{-T}\boldsymbol{\Lambda} \tag{42}$$

with $\mathbf{A}^{-1} = \mathbf{I} - \frac{1}{J}\left[\mathbf{a} \otimes \mathbf{d}_3(s,t)\right]$.

The material time derivative of the location of a material point in the current configuration reads

$$\dot{\mathbf{x}}(X^k, s, t) = \dot{\boldsymbol{\varphi}}(s,t) + X^k \dot{\mathbf{d}}_k(s,t), \tag{43}$$

by which the time derivative of deformation gradient can be evaluated with

$$\begin{aligned}\dot{\mathbf{F}}(X^1, X^2, s, t) &= \frac{\partial \dot{\mathbf{x}}}{\partial \mathbf{X}} = \frac{\partial \dot{\mathbf{x}}}{\partial X_i} \otimes \mathbf{d}_i(s,0) \\ &= \dot{\mathbf{d}}_1(s,t) \otimes \mathbf{d}_1(s,0) + \dot{\mathbf{d}}_2(s,t) \otimes \mathbf{d}_2(s,0) \\ &\quad + \left(\frac{\partial \dot{\boldsymbol{\varphi}}(s,t)}{\partial s} + X^1 \frac{\partial \dot{\mathbf{d}}_1(s,t)}{\partial s} + X^2 \frac{\partial \dot{\mathbf{d}}_2(s,t)}{\partial s}\right) \otimes \mathbf{d}_3(s,0) \\ &= \dot{\boldsymbol{\Lambda}}(s) + \left(\frac{\partial \dot{\boldsymbol{\varphi}}(s,t)}{\partial s} - \dot{\mathbf{d}}_3(s,t) + X^1 \frac{\partial \dot{\mathbf{d}}_1(s,t)}{\partial s} \right. \\ &\quad \left. + X^2 \frac{\partial \dot{\mathbf{d}}_2(s,t)}{\partial s}\right) \otimes \mathbf{d}_3(s,0).\end{aligned} \tag{44}$$

4.2 Electrical kinematics in the beam

To formulate the electromechanical coupling problem, the electric potential will serve as the extra degree of freedom. In this work, the electric potential at the point (X^1, X^2, s) is represented by the electric potential at the beam node plus the increment from the beam node to the point (X^1, X^2) on the cross section as shown in Fig. 2. Similar to the local description of the cross section in Eq. (13), the electric potential on the cross section is given by

$$\phi(X^1, X^2, s) = \phi_o(s) + X^1 \alpha(s) + X^2 \beta(s) \tag{45}$$

with $\phi_o(s)$ the electric potential at the beam node, $\alpha(s)$ and $\beta(s)$ the incremental parameters of the electric potential in the directions of $\mathbf{d}_1$ and $\mathbf{d}_2$, respectively. Equation (45) is the linear part of a Taylor series expansion of the electric potential. To be able to generate complex beam deformations via dielectric actuator, at least a linear distribution of electric potential on the beam cross section is required. The extension to nonlinear distributions of the electric potential on beam cross section can be made by adding the higher order terms.

The Eq. (13) describes the cross section as a plane. Correspondingly, Eq. (45) defines a linear distribution of electric potential on the cross section. If the electric potential is constant within the cross section (i.e. $\alpha, \beta = 0$), the electric field only exists in the $\mathbf{d}_3$ direction, which will lead to the uniaxial contraction in beam.

According to the Maxwell equations, the electric field is defined as the gradient of the electric potential ϕ, see Eq. (9). To compute the gradient of the electric potential for the beam, a similar approach as the deformation gradient in Eq. (34) can be adopted. By applying the electric potential in

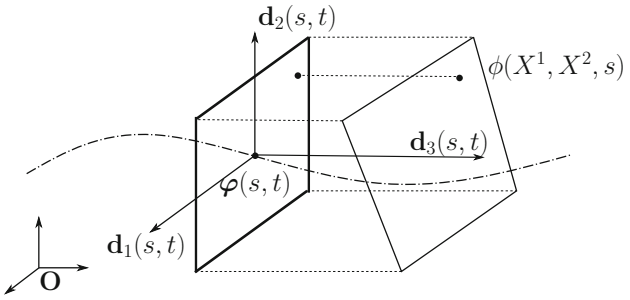

Fig. 2 Linear distribution of electric potential on cross section

Eq. (45), the electric field at (X^1, X^2, s) in the beam can be computed as

$$\mathbf{E}^e(X^1, X^2, s) = -\frac{\partial \phi}{\partial X_i} \otimes \mathbf{d}_i(s,0) \tag{46}$$

$$= -\left[\alpha(s)\mathbf{d}_1(s,0) + \beta(s)\mathbf{d}_2(s,0) + \left(\frac{\partial \phi_o(s)}{\partial s} + X^1\frac{\partial \alpha(s)}{\partial s} + X^2\frac{\partial \beta(s)}{\partial s}\right)\mathbf{d}_3(s,0)\right]. \tag{47}$$

For the later computing of the virtual work induced by the electric field, the variation of the electric field is given by

$$\delta\mathbf{E}^e = -\left[\delta\alpha(s)\mathbf{d}_1(s,0) + \delta\beta(s)\mathbf{d}_2(s,0) + \delta\left(\frac{\partial \phi_o(s)}{\partial s} + X^1\frac{\partial \alpha(s)}{\partial s} + X^2\frac{\partial \beta(s)}{\partial s}\right)\mathbf{d}_3(s,0)\right]. \tag{48}$$

Since the electric field expressed in Eq. (47) is not a strain-like variable for beam, we need to formulate the strain-like electrical variable $\boldsymbol{\varepsilon}$, which can be consistently conjugated with the beam electric displacement $\mathbf{d}^e$ in Eq. (29). For this purpose, we start from the internal virtual work δW_{int} induced by the electric field in the 3D continuum

$$\delta W_{\text{int}} = \int_{B_0} \mathbf{D} \cdot \delta\mathbf{E}^e dV. \tag{49}$$

By applying the electric displacement and the variation of electric field in Eq. (48) to the internal virtual work, we obtain

$$\delta W_{int} = \int_{B_0} -(D_i\mathbf{d}_i)\cdot\left[\delta\alpha(s)\mathbf{d}_1(s,0) + \delta\beta(s)\mathbf{d}_2(s,0) + \delta\left(\frac{\partial \phi_o(s)}{\partial s} + X^1\frac{\partial \alpha(s)}{\partial s} + X^2\frac{\partial \beta(s)}{\partial s}\right)\mathbf{d}_3(s,0)\right]dV$$

$$= \int_c -\left[\delta\alpha(s)\int_\Sigma D_1 dA + \delta\beta(s)\int_\Sigma D_2 dA + \delta\frac{\partial \phi_o(s)}{\partial s}\int_\Sigma D_3 dA + \delta\frac{\partial \alpha(s)}{\partial s}\int_\Sigma X^1 D_3 dA + \delta\frac{\partial \beta(s)}{\partial s}\int_\Sigma X^2 D_3 dA\right]ds. \tag{50}$$

Due to the presence of the cross section coordinates X^1 and X^2 in Eq. (50), any strain-like electrical variable depends on the cross section at s. However, assuming that $\alpha(s)$ and $\beta(s)$ are linear functions in terms of s, the variations of $\frac{\partial \alpha(s)}{\partial s}$ and $\frac{\partial \beta(s)}{\partial s}$ vanish leading to the following expression for the virtual work

$$\delta W_{int} = \int_c -\left[\delta\alpha(s)\int_\Sigma D_1 dA + \delta\beta(s)\int_\Sigma D_2 dA + \delta\frac{\partial \phi_o(s)}{\partial s}\int_\Sigma D_3 dA\right]ds = \int_c \mathbf{d}^e \cdot \delta\boldsymbol{\varepsilon} ds, \tag{51}$$

where the work conjugate of $\mathbf{d}^e$ and $\boldsymbol{\varepsilon}$ can be observed with the strain-like electrical variable $\boldsymbol{\varepsilon}$ defined as

$$\boldsymbol{\varepsilon} = \left[-\alpha(s)\ -\beta(s)\ -\frac{\partial \phi_o(s)}{\partial s}\right]^T. \tag{52}$$

5 Strain energy function for the beam

The strain energy function of the beam model has been derived for the hyperelastic constitutive law, such as the widely used Saint-Venant–Kirchhoff model [28]. However, the strain energy for other material behaviors are not given for the beam model, including the dielectric elasticity. In continuum electromechanics, many material models have been postulated to describe different material behaviors, such as the dielectric elastomers in [33]. To apply these material models in a beam formulation, the rewriting of the strain energy function in terms of the beam strains is required, which can be achieved by applying the kinematic relations introduced in Sect. 4. In this part, we firstly present the derivation of the widely used Saint-Venant–Kirchhoff model for the beam. Then, the strain energy function of the dielectric elastomer is formulated for the beam such that it can be used in the beam constitutive equations directly.

5.1 Saint-Venant–Kirchhoff model

The Saint-Venant–Kirchhoff model describes a linear relationship between the Green-Lagrange strain $\mathbf{E}$ and the second Piola–Kirchhoff stress $\mathbf{S}$ with the strain energy function

$$\Omega(\mathbf{E}) = \frac{1}{2}\lambda\,(\text{tr}\mathbf{E})^2 + \mu\mathbf{E} : \mathbf{E}, \tag{53}$$

in which λ and μ are the Lamé parameters. Inserting the linear part of $\mathbf{E}$ in Eq. (41) into the previous equation, the reduced strain energy Ω^r reads

$$\Omega^r = \frac{1}{2}\left\{\lambda\left[\mathrm{tr}(\mathbf{a}^r \otimes \mathbf{d}_3(s,0))^{\mathrm{sym}}\right]^2 + 2\mu\left[\frac{1}{2}(\mathbf{a}^r \cdot \mathbf{d}_3(s,0))^2 + \frac{1}{2}\mathbf{a}^r \cdot \mathbf{a}^r\right]\right\} = \frac{1}{2}\mathbf{a}^{rT}\mathbf{D}\mathbf{a}^r \tag{54}$$

with $\mathbf{D} = (\lambda+\mu)\mathbf{d}_3(s,0)\otimes\mathbf{d}_3(s,0) + \mu\mathbf{I}$. Integrating Ω^r over beam cross section, the reduced strain energy for the beam is obtained as

$$\begin{aligned}\Omega_b^r(\boldsymbol{\Gamma},\mathbf{K}) &= \int_\Sigma \Omega^r dA \\ &= \frac{1}{2}\int_\Sigma (\boldsymbol{\Gamma} + \mathbf{K}\times\mathbf{r})^T\mathbf{D}(\boldsymbol{\Gamma}+\mathbf{K}\times\mathbf{r})dA \\ &= \frac{1}{2}\boldsymbol{\Gamma}^T\mathbf{D}^N\boldsymbol{\Gamma} + \frac{1}{2}\mathbf{K}^T\mathbf{D}^K\mathbf{K},\end{aligned} \tag{55}$$

where the material tangents $\mathbf{D}^N$ and $\mathbf{D}^K$ are given by

$$\mathbf{D}^N = \begin{bmatrix}\mu A & 0 & 0\\ 0 & \mu A & 0\\ 0 & 0 & (\lambda+2\mu)A\end{bmatrix},$$
$$\mathbf{D}^K = \begin{bmatrix}(\lambda+2\mu)J_{22} & (\lambda+2\mu)J_{12} & 0\\ (\lambda+2\mu)J_{21} & (\lambda+2\mu)J_{11} & 0\\ 0 & 0 & \mu J_p\end{bmatrix} \tag{56}$$

with the first moments of area $J_{ii} = \int_\Sigma X_i X_i dA$, the product moments of area $J_{12} = J_{21} = -\int_\Sigma X_1 X_2 dA$ and the polar moment of area $J_p = \int_\Sigma X_1^2 + X_2^2 dA$. It can be observed that the widely used beam constitutive model postulated by [28,29] are recovered when $\lambda + 2\mu = E$. According to the formula of Lamé parameters, this formulation assumes the limit of Poisson's $\nu \to 0$, i.e. no lateral contraction. However, the physics is incorrect and it leads to the incorrect material moduli. To overcome this problem, the uniaxial stress assumption can be additionally included within a mix formulation such as the Hellinger-Reissner principle. An alternative solution is to apply a very small Poisson's ratio ν in the simulation, by which a relatively fair comparison between the beam model and the 3D finite element model can be achieved as shown in the numerical examples of this work.

Since the reduced beam strain energy Ω_b^r is derived by only inserting the linear part of the Green-Lagrange strain $\mathbf{E}$, the derived beam force will be just the linear part of the full one. To explain it, we start from the current force $\mathbf{n}$ of the beam computed from the first Piola–Kirchhoff stress $\mathbf{P}$

$$\begin{aligned}\mathbf{n} &= \int_\Sigma \mathbf{P}\mathbf{d}_3(s,0)dA = \int_\Sigma \mathbf{F}\mathbf{S}\mathbf{d}_3(s,0)dA \\ &= \int_\Sigma \boldsymbol{\Lambda}\left[\mathbf{I} + \mathbf{a}^r\otimes\mathbf{d}_3(s,0)\right]\mathbf{S}\mathbf{d}_3(s,0)dA.\end{aligned} \tag{57}$$

By applying the relation $\mathbf{n} = \boldsymbol{\Lambda}\mathbf{N}$, the reference beam force $\mathbf{N}$ reads

$$\mathbf{N} = \int_\Sigma \left[\mathbf{I} + \mathbf{a}^r\otimes\mathbf{d}_3(s,0)\right]\mathbf{S}\mathbf{d}_3(s,0)dA. \tag{58}$$

It can be observed that force $\mathbf{N}$ is composed of two parts, one depending only on the stress and another also depending on strain variable $\mathbf{a}^r$. It has been proven that $\mathbf{N}$ is work conjugated with the beam strain $\boldsymbol{\Gamma}$, see the details in [4]. When the reduced strain energy in Eq. (55) is applied, the derived force $\mathbf{N}^r$ equals to the integration of the second Piola–Kirchhoff stress $\mathbf{S}^{\mathrm{lin}}$ computed with the linear strain $\mathbf{E}^{\mathrm{lin}}$

$$\mathbf{N}^r = \frac{\partial\Omega_b^r}{\partial\boldsymbol{\Gamma}} = \int_\Sigma \mathbf{S}^{\mathrm{lin}}\mathbf{d}_3(s,0)dA, \tag{59}$$

which can be seen as the linear part of the full force $\mathbf{N}$ in Eq. (58).

5.2 Extended Neo-Hookean model for DEA

To model the DEA, the material model of the dielectric elasticity applied in [24] for the finite element simulation is applied to the beam model in this work, where the strain energy density is given by

$$\begin{aligned}\Omega(\mathbf{C},\mathbf{E}^e) = &\underbrace{\frac{\mu}{2}(\mathbf{C}:\mathbf{1}-3) - \mu\ln J + \frac{\lambda}{2}(\ln J)^2}_{\text{Neo-Hookean}} \\ &+ \underbrace{c_1\mathbf{E}^e\cdot\mathbf{E}^e + c_2\mathbf{C}:(\mathbf{E}^e\otimes\mathbf{E}^e)}_{\text{Polarization in dielectric material}} \\ &- \underbrace{\frac{1}{2}\varepsilon_0 J\mathbf{C}^{-1}:(\mathbf{E}^e\otimes\mathbf{E}^e)}_{\text{Free space term in vacuum}}\end{aligned} \tag{60}$$

with ε_0 the vacuum permittivity, c_1 and c_2 the electrical parameters. It can be observed that the strain energy is composed of three parts, the Neo-Hookean part referring to the pure elastic behavior, the polarization part referring to the polarization in the condensed matter and the free space part referring to the effect in vacuum. The last two terms in Eq. (60) characterize the electromechanical coupling.

Apart from the dielectric elasticity, the viscoelastic effect in the dielectric material is accounted for by means of the first Piola–Kirchhoff stress $\mathbf{P}^{\mathrm{vis}}$, see the Kelvin–Voigt model in [35],

$$\mathbf{P}^{\mathrm{vis}} = \frac{1}{2}J\eta\left(\mathbf{F}^{-T}\cdot\dot{\mathbf{F}}^T\cdot\mathbf{F}^{-T} + \dot{\mathbf{F}}\cdot\mathbf{C}^{-1}\right), \tag{61}$$

in which η is the damping parameter.

The strain energy function for the beam corresponding to the continuum model in Eq. (60) can be derived with the

same procedure as the Saint-Venant–Kirchhoff model. Since the coefficient ε_0 has a very small value, see Table 1, the free space term in Eq. (60) is neglected in this work. The strain energy function for beam is obtained by integrating $\Omega(\mathbf{C}, \mathbf{E}^e)$ over the cross section

$$\Omega_b(\boldsymbol{\Gamma}, \mathbf{K}, \boldsymbol{\varepsilon}) = \int_\Sigma \Omega(\mathbf{C}, \mathbf{E}^e) dA, \tag{62}$$

where the integration can be evaluated with the numerical approach as well as the analytical approach. As the analytical approach, the beam strain energy function Ω_b is explicitly formulated in the "Appendix". For the sake of simplicity, the logarithm term in the beam strain energy function is approximated by using the first two terms of its Taylor series expansion, see Eq. (90). The higher order terms can be added in the approximation if needed.

6 Discrete variational integration scheme with null space projection

6.1 Discrete Euler–Lagrange equations

In this work, the electromechanically coupled beam dynamics is approximated within the constrained discrete variational scheme with the null space projection. The Lagrange–d'Alembert principle in Eq. (14) can be extended to constrained systems by enforcing the constraints via Lagrange multipliers as

$$\delta \int_0^T \left[L(\mathbf{q}, \dot{\mathbf{q}}) - \mathbf{g}^T(\mathbf{q}) \cdot \boldsymbol{\lambda} \right] dt + \int_0^T \mathbf{f}^{\text{ext}}(t) \cdot \delta \mathbf{q} dt = 0, \tag{63}$$

where $\mathbf{q}$ is the configuration, $L(\mathbf{q}, \dot{\mathbf{q}})$ is the Lagrangian, $\mathbf{g}$ represents holonomic constraints, $\boldsymbol{\lambda}$ is the Lagrangian multiplier and $\mathbf{f}^{\text{ext}}(t)$ is the external force. By considering the electrical effect in geometrically exact beam, the electric potential ϕ_o and the incremental variables (α, β) in Eq. (45) are treated as the electrical degrees of freedom $\boldsymbol{\phi} = \left[\phi_o \ \alpha \ \beta\right]$ such that the configuration of the beam model is extended to

$$\mathbf{q} = \left[\boldsymbol{\varphi} \ \mathbf{d}_1 \ \mathbf{d}_2 \ \mathbf{d}_3 \ \boldsymbol{\phi}\right]^T. \tag{64}$$

According to the kinematic assumptions in geometrically exact beams, the directors have to fulfill the orthogonal constraints

$$\mathbf{g}(\mathbf{q}) = \begin{bmatrix} \frac{1}{2}(\mathbf{d}_1^T \mathbf{d}_1 - 1) \\ \frac{1}{2}(\mathbf{d}_2^T \mathbf{d}_2 - 1) \\ \frac{1}{2}(\mathbf{d}_3^T \mathbf{d}_3 - 1) \\ \mathbf{d}_1^T \mathbf{d}_2 \\ \mathbf{d}_1^T \mathbf{d}_3 \\ \mathbf{d}_2^T \mathbf{d}_3 \end{bmatrix} = \mathbf{0}. \tag{65}$$

The continuous Lagrangian contains the difference between the kinetic energy $T(\dot{\mathbf{q}})$ and the internal potential energy $V(\mathbf{q})$

$$L(\mathbf{q}, \dot{\mathbf{q}}) = T(\dot{\mathbf{q}}) - V(\mathbf{q}). \tag{66}$$

Since the electrical variables do not contribute to the kinetic energy, the kinetic energy for geometrically exact beams is computed as

$$T = \int_c \left(\frac{1}{2} A_\rho \left| \dot{\boldsymbol{\varphi}} \right|^2 + \frac{1}{2} \sum_{i=1}^{2} M_\rho^i \left| \dot{\mathbf{d}}_i \right|^2 \right) ds, \tag{67}$$

where A_ρ is the mass density per reference arc-length and M_ρ^i are the principle mass moments of inertia of cross section. In accordance with the configuration defined in Eq. (64), the component of the consistent mass matrix corresponding to the electrical degree of freedom $\boldsymbol{\phi}$ will be zero.

For the coupled hyperelastic material in DEA, the internal potential energy is computed by an integration of the beam strain energy density Ω_b in Eq. (62) over the beam center line

$$V(\mathbf{q}) = \int_c \Omega_b(s) ds. \tag{68}$$

The external force $\mathbf{f}^{\text{ext}}$ contains all non-conservative forces, such as the viscoelastic effect in this work. Based on the Kelvin–Voigt model in Eq. (61), the non-conservative work contributed by the viscoelastic effect is given by

$$W^{\text{vis}} = \int_{B_0} \mathbf{P}^{\text{vis}} : \mathbf{F} dV, \tag{69}$$

where the work is computed from the two conjugate quantities being the first Piola–Kirchhoff stress $\mathbf{P}^{\text{vis}}$ from the Kelvin–Voigt model and the deformation gradient $\mathbf{F}$. In this case, the external force corresponding to the viscoelastic effect can be formulated as

$$\mathbf{f}^{\text{vis}}(\mathbf{q}, \dot{\mathbf{q}}) = \frac{\partial W^{\text{vis}}}{\partial \mathbf{q}} = \int_{B_0} \frac{\partial W^{\text{vis}}}{\partial \mathbf{F}} : \frac{\partial \mathbf{F}}{\partial \mathbf{q}} dV = \int_c \int_\Sigma \mathbf{P}^{\text{vis}} : \frac{\partial \mathbf{F}}{\partial \mathbf{q}} dA ds. \tag{70}$$

The beam is first spatially discretized with the 1D finite elements, where one-dimensional Lagrange-type linear shape functions are applied in the discretization of beam configuration $\mathbf{q}$ in Eq. (64). In this case, the beam directors are directly discretized in space together with the beam centroids, see [22] for instance. Then the variational integration scheme, see e.g. [16], is applied to temporally discretize the action of the dynamic system, by which the good long term energy behavior can be obtained. In the variational integration scheme, the action integral within the time interval (t_n, t_{n+1}) is approximated with the discrete Lagrangian L_d as

$$\int_{t_n}^{t_{n+1}} L(\mathbf{q}, \dot{\mathbf{q}})dt \approx L_d(\mathbf{q}_n, \mathbf{q}_{n+1}) = \Delta t L(\frac{\mathbf{q}_{n+1}+\mathbf{q}_n}{2}, \frac{\mathbf{q}_{n+1}-\mathbf{q}_n}{\Delta t}), \tag{71}$$

where the discrete Lagrangian L_d is computed by applying the finite difference approximation to the velocity $\dot{\mathbf{q}}$ and the midpoint rule to the configuration $\mathbf{q}$, i.e.

$$\dot{\mathbf{q}} \approx \frac{\mathbf{q}_{n+1}-\mathbf{q}_n}{\Delta t}, \qquad \mathbf{q} \approx \frac{\mathbf{q}_{n+1}+\mathbf{q}_n}{2}. \tag{72}$$

After the temporal discretization, the discrete Euler–Lagrange equations can be obtained by taking the variation of the discrete action and requiring stationarity. To eliminate the constraint forces $\boldsymbol{\lambda}$ from the system, see e.g. [6], the nodal reparametrization $\mathbf{q}_{n+1} = \mathbf{F}_d(\mathbf{u}_{n+1}, \mathbf{q}_n)$ and the discrete null space matrix $\mathbf{P}_d$ are applied to the discrete Euler–Lagrange equations leading to

$$\mathbf{P}_d^T(\mathbf{q}_n)\left[\frac{\partial L_d(\mathbf{q}_{n-1}, \mathbf{q}_n)}{\partial \mathbf{q}_n} + \frac{\partial L_d(\mathbf{q}_n, \mathbf{F}_d(\mathbf{u}_{n+1}, \mathbf{q}_n))}{\partial \mathbf{q}_n} + \mathbf{f}_n^{\text{ext}-} + \mathbf{f}_{n-1}^{\text{ext}+}\right] = \mathbf{0}, \tag{73}$$

where $\mathbf{u}_{n+1}$ is the generalized configuration acting as the unknown variable, $\mathbf{f}_n^{\text{ext}-}$ and $\mathbf{f}_{n-1}^{\text{ext}+}$ are the discrete generalized external forces evaluated as

$$\mathbf{f}_n^{\text{ext}-} = \frac{\Delta t}{2}\mathbf{f}^{\text{vis}}\left(\frac{\mathbf{q}_{n+1}+\mathbf{q}_n}{2}, \frac{\mathbf{q}_{n+1}-\mathbf{q}_n}{\Delta t}\right),$$
$$\mathbf{f}_{n-1}^{\text{ext}+} = \frac{\Delta t}{2}\mathbf{f}^{\text{vis}}\left(\frac{\mathbf{q}_{n-1}+\mathbf{q}_n}{2}, \frac{\mathbf{q}_{n-1}-\mathbf{q}_n}{\Delta t}\right). \tag{74}$$

6.2 Null space matrix and parametrization of rotations

The internal null space matrix $\mathbf{P}_{\text{int}}$ can be found by expressing the redundant velocity $\dot{\mathbf{q}} \in \mathbb{R}^{15}$ in terms of the generalized velocity $\mathbf{t} \in \mathbb{R}^9$

$$\dot{\mathbf{q}} = \mathbf{P}_{\text{int}}(\mathbf{q}) \cdot \mathbf{t}, \tag{75}$$

where the generalized velocity is composed of the translational velocity $\dot{\boldsymbol{\varphi}}$, the angular velocity $\boldsymbol{\omega}$ and the velocity of electric potential $\dot{\boldsymbol{\phi}}$, i.e. $\mathbf{t} = \left[\dot{\boldsymbol{\varphi}}\ \boldsymbol{\omega}\ \dot{\boldsymbol{\phi}}\right]^T$. The corresponding internal null space matrix at time t_n is written as

$$\mathbf{P}_{\text{int}}(\mathbf{q}_n) = \begin{bmatrix} \mathbf{I} & \mathbf{0} & \mathbf{0} \\ \mathbf{0} & -\hat{\mathbf{d}}_{1,n} & \mathbf{0} \\ \mathbf{0} & -\hat{\mathbf{d}}_{2,n} & \mathbf{0} \\ \mathbf{0} & -\hat{\mathbf{d}}_{3,n} & \mathbf{0} \\ \mathbf{0} & \mathbf{0} & \mathbf{I} \end{bmatrix}, \tag{76}$$

where $\hat{\mathbf{d}}_{i,n}$ denotes the skew-symmetric matrix corresponding to the director vector $\mathbf{d}_{i,n}$ at t_n and $\mathbf{I}$ is the 3 by 3 identity matrix. For a multibody dynamic system composed of flexible beam actuators, rigid bodies, joints and constraints, the null space matrix can be designed by considering the electric potential as extra degree of freedom as well.

To solve the discrete Euler–Lagrange equations efficiently, the system can be reduced further into the minimal possible dimensions by use of the nodal reparametrization, which can be achieved by introducing a rotation matrix $\mathbf{R}(\boldsymbol{\theta})$ parametrized in terms of the rotational variable $\boldsymbol{\theta}$. The rotation matrix can be chosen as the exponential map, see e.g. [18],

$$\mathbf{R}(\boldsymbol{\theta}) = \exp(\hat{\boldsymbol{\theta}}) = \mathbf{I} + \frac{\sin\|\boldsymbol{\theta}\|}{\|\boldsymbol{\theta}\|}\hat{\boldsymbol{\theta}} + \frac{1}{2}\left(\frac{\sin\|\boldsymbol{\theta}\|/2}{\|\boldsymbol{\theta}\|/2}\right)^2(\hat{\boldsymbol{\theta}})^2. \tag{77}$$

The generalized configuration of the electromechanically coupled beam is specified by

$$\mathbf{u} = \left[\mathbf{u}_\varphi\ \boldsymbol{\theta}\ \mathbf{v}\right]^T \tag{78}$$

with $\mathbf{u}_\varphi, \boldsymbol{\theta}$ and $\mathbf{v}$ characterizing the incremental displacement, the incremental rotation and the incremental electric potential, respectively. In this case, the nodal configuration for the next time step can be updated as

$$\mathbf{q}_{n+1} = \mathbf{F}_d(\mathbf{u}_{n+1}, \mathbf{q}_n) = \begin{bmatrix} \boldsymbol{\varphi}_n + \mathbf{u}_\varphi \\ \exp(\hat{\boldsymbol{\theta}}) \cdot \mathbf{d}_{1,n} \\ \exp(\hat{\boldsymbol{\theta}}) \cdot \mathbf{d}_{2,n} \\ \exp(\hat{\boldsymbol{\theta}}) \cdot \mathbf{d}_{3,n} \\ \boldsymbol{\phi} + \mathbf{v} \end{bmatrix}. \tag{79}$$

6.3 Tangent matrix

By means of the nodal reparametrization, the unknowns of the equations system in Eq. (73) is changed from $\mathbf{q}_{n+1}$ to the generalized variables $\mathbf{u}_{n+1}$. The nonlinear equation system is solved by use of the Newton-Rapson algorithm with the tangent matrix at iteration i

$$\mathbf{K}_T^i = \mathbf{P}^T(\mathbf{q}_n)\frac{\partial \mathbf{R}^L(\mathbf{q}_{n+1}^i)}{\partial \mathbf{q}_{n+1}^i}\frac{\partial \mathbf{q}_{n+1}(\mathbf{u}_{n+1}^i)}{\partial \mathbf{u}_{n+1}^i}, \tag{80}$$

in which $\mathbf{R}^L(\mathbf{q}_{n+1})$ is the residual of the discrete Euler–Lagrange equation. When boundary conditions are imposed on some degrees of freedom of a beam node, the corresponding components in null space matrix will be zero. By crossing out the rows involved in boundary conditions, the non-singular tangent matrix can be obtained. Accordingly, the boundary conditions can be imposed by setting specific incremental values in the update of the nodal configuration in Eq. (79). In this work, the residual vector and the tangent matrix are derived by using the automatic differentiation tool CasADi [1].

6.4 Legendre transformation for energy evaluation and system initialization

Since the velocity involved in the kinetic energy is approximated with the finite difference scheme, it does not fulfill the hidden constraints and their time derivatives exactly. An alternative energy formulation is the discrete Hamiltonian evaluated with the momentum, which can be obtained via the discrete Legendre transformation, see e.g. [16]. Since the consistent mass matrix corresponding to the kinetic energy in Eq. (67) is singular, it can not be applied to compute the Hamiltonian directly where the inverse of the mass matrix is required. Due to the fact that the kinetic energy is independent of the rate of $\mathbf{d}_3$ and the rate of electric potential, a reduced non-singular mass matrix $\bar{\mathbf{M}}$ can be defined at node s as

$$\bar{\mathbf{M}} = \begin{bmatrix} A_\rho \mathbf{I} & \mathbf{0} & \mathbf{0} \\ \mathbf{0} & M_\rho^1 \mathbf{I} & \mathbf{0} \\ \mathbf{0} & \mathbf{0} & M_\rho^2 \mathbf{I} \end{bmatrix} \tag{81}$$

with $\mathbf{I}$ the 3×3 identity matrix. Therefore, the discrete Hamiltonian can be evaluated with the reduced mass matrix $\bar{\mathbf{M}}$ and its conjugated reduced momentum

$$\bar{\mathbf{p}} = [\mathbf{p}_\varphi, \mathbf{p}_1, \mathbf{p}_2]^T. \tag{82}$$

To eliminate the Lagrangian multiplier term from the reduced momentum $\bar{\mathbf{p}}$, the projected discrete Legendre transformation can be applied. In this case, the projected reduced momentum can be computed as

$${}^Q\bar{\mathbf{p}}_n^- = -\bar{\mathbf{Q}}(\mathbf{q}_n)\frac{\partial L_d(\mathbf{q}_n, \mathbf{q}_{n+1})}{\partial \bar{\mathbf{q}}_n}, \tag{83}$$

where ${}^Q\bar{\mathbf{p}}_n^-$ is the reduced momentum at time t_n, $\bar{\mathbf{Q}}$ is the projection matrix and $\bar{\mathbf{q}}_n$ is the vector containing the first 9 elements of $\mathbf{q}_n$. Corresponding to the reduced momentum ${}^Q\bar{\mathbf{p}}_n^-$ and the mass matrix $\bar{\mathbf{M}}$, the projection matrix is computed in the reduced form

$$\bar{\mathbf{Q}} = \mathbf{I}_{9\times 9} - \bar{\mathbf{G}}^T(\bar{\mathbf{G}}\bar{\mathbf{M}}^{-1}\bar{\mathbf{G}}^T)^{-1}\bar{\mathbf{G}}\bar{\mathbf{M}}^{-1} \tag{84}$$

with the reduced internal constraint Jacobi matrix $\bar{\mathbf{G}}_{3\times 9}$ given by

$$\bar{\mathbf{G}} = \begin{bmatrix} \mathbf{0} & \mathbf{d}_1^T & \mathbf{0} \\ \mathbf{0} & \mathbf{0} & \mathbf{d}_2^T \\ \mathbf{0} & \mathbf{d}_2^T & \mathbf{d}_1^T \end{bmatrix}. \tag{85}$$

The discrete Hamiltonian H_d can be computed as

$$H_d = \int_c \left(\frac{1}{2}{}^Q\bar{\mathbf{p}}_n^{-T}\cdot\bar{\mathbf{M}}^{-1}\cdot{}^Q\bar{\mathbf{p}}_n^-\right)ds + V(\mathbf{q}_n). \tag{86}$$

Furthermore, the discrete Legendre transformation is applied to initialize the system at time step t_0. In the discrete Euler–Lagrange equation (73), the unknown value of $\mathbf{q}_{-1}$ is required to solve $\mathbf{q}_1$. To avoid the computation of $\mathbf{q}_{-1}$, the discrete momentum obtained from the Legendre transformation is initialized with an initial momentum $\mathbf{p}_0^- = \mathbf{p}(0)$, which leads to the equation of motion at t_0

$$\mathbf{P}^T(\mathbf{q}_0)\left[-\frac{\partial L_d(\mathbf{q}_0, \mathbf{q}_1)}{\partial \mathbf{q}_0} - \mathbf{f}_0^{\text{ext}-}\right] = \mathbf{P}^T(\mathbf{q}_0)\mathbf{p}(0). \tag{87}$$

In this case, $\mathbf{q}_1$ can be computed given $\mathbf{q}_0 = \mathbf{q}(0)$ and $\mathbf{p}(0)$.

7 Numerical examples

The material parameters of the dielectric elastomer applied in this work are shown in Table 1. Instead of using the Lamé parameter $\mu = 0.233$ Mpa in [24] for the nearly incompressible case, the Lamé parameter μ is set to be 233 Mpa in this work for the sake of a smaller Poisson's ratio. According to the discussions in Sect. 5.1, the smaller Poisson's ratio allows the better comparison of 3D FEM model with the beam model with assumption of no lateral contractions.

The geometry of the beam with length l and square cross section $b \times b$ is shown in Fig. 3. The beam is composed of N_c stacked DEA cells, where the thickness of the electrode connecting two adjacent cells is neglected, thus the beam is fully composed of the dielectric elastomer. Each DEA cell is

Table 1 Material parameters

ρ g/mm^3	λ Mpa	μ Mpa	ε_0 C/Vm	c_1 N/V^2	c_2 N/V^2
1	999.8	233	8.854×10^{-12}	5×10^{-8}	1×10^{-9}

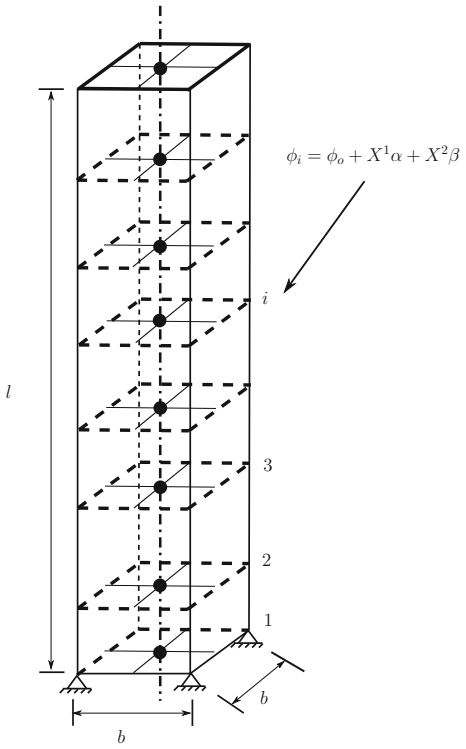

Fig. 3 Boundary conditions on the beam

discretized with N_e finite elements. The bottom beam node is fixed and the electrical boundary conditions ϕ_i are imposed on the beam nodes corresponding to the electrodes i. The contractions of DEA cells will lead to different deformations in the beam, including uniaxial contraction, shear, bending and torsion. The electrical boundary conditions and the beam size for generating different beam deformations in this work are given in Table 2.

7.1 Uniaxial contraction

To generate the uniaxial contraction in the beam, the uniform electric potential is applied on the cross section, i.e. $\alpha, \beta = 0$. As shown in Table 2, the beam is composed of one ($N_c = 1$) DEA cell and the electric potentials $\phi_1 = 0$ V and $\phi_2 = 2 \times 10^4$ V are applied to the two electrodes of the beam DEA cell, respectively. The motion of the beam discretized with $N_e = 5$ elements, i.e. 6 nodes, is computed with the time step of 1×10^{-4} ms.

Due to the contractive forces from the dielectric effect, the vibration of the beam is induced as shown in Fig. 4, where the position X_z of the beam node at the free end is depicted. In Fig. 4a, the beam strain energy Ω_b derived in the "Appendix" is compared with that evaluated by the numerical integration over cross section. The derived strain energy shows good agreement with the numerical model in Fig. 4a and will be applied in the following parts. In Fig. 4b, the damping effect with different values of the viscosity parameter η is depicted. Without viscosity i.e. $\eta = 0$, the vibration of the beam continues over time. With the increase of viscoelastic effect, the increase of damping effect on the beam can be observed. By setting $\eta = 0.5$, the viscoelastic beam is gradually approaching a static state.

To evaluate the energy property of the beam, the discrete Hamiltonian H_d computed with momentum is plotted in Fig. 5. As shown in Fig. 5a, the total energy oscillates around a value when there is no viscosity i.e. $\eta = 0$. By introducing the viscosity, the total energy decreases at the beginning stage and then preserves a smaller value, where the decrease of total energy is induced by the decrease of kinetic energy. Additionally, with the increase of the damping parameter η, the total energy decreases faster. To evaluate the energy behavior for $\eta = 0$ further, the kinetic energy T_d and the potential energy V_d corresponding to the total energy H_d are plotted in Fig. 5b. It can be observed that the frequency of the kinetic energy is twice as much as the frequency of the displacement in Fig. 4, which is reasonable by considering the velocity changes. However, the potential energy shares the same frequency with the kinetic energy, which is different from the pure elastic case where the elastic potential energy shares the same frequency with displacement. The reason can be attributed to the fact that the potential energy of the dielectric elastomer holding its maximum value in the undeformed state decreases to a minimum value in an intermediate compressed state, and then increases with the further compression, see the first V-shape oscillation of V_d in Fig. 5b.

The magnitude of contractions of the beam depends on the magnitude of electric potential applied on it. With the increase of electric potential, the increase of contraction can be observed as shown in the upper graph of Fig. 6. To validate the beam model, the contractions of the beam model are compared with the results of the 3D FEM model as shown in the lower graph of Fig. 6. In the 3D FEM model, the beam structure is discretized with 5 elements in longitudinal direction whereas with 2×2 elements for the cross section, where the same material model and size as the beam model are applied. Since the same constitutive model is applied in the beam model and the 3D FEM model, the zero normal stress conditions in the transversal directions are fulfilled in the same extent in both cases. However, the lateral deformations still exist in the 3D FEM model, thus the inextensibility condition is not fulfilled while it is always fulfilled in the beam model. For the uniaxial contraction considered in this section, the inextensibility condition is additionally imposed

Table 2 Electrical boundary conditions and beam size

	ϕ_i/V	ϕ_o	α	β	N_c	b/mm	l/mm
Contraction	ϕ_o at $i = 2$	$2e4$	0	0	1	0.02	0.1
Bending	0 at $i = 1, 3...$; $\phi_o + \alpha X^1 + \beta X^2$ at $i = 2, 4, ...$	$2e2$	$2e4$	0	40	0.005	0.1
Shear	$\phi_o + i4e2 + \alpha X^1 + \beta X^2$	$2e2$	$2e4$	0	20	0.005	0.05
Torsion	$\phi_o + \alpha(cos\theta_i - sin\theta_i)X^1 + \beta(cos\theta_i + sin\theta_i)X^2$	$2e3$	$5e4$	$5e4$	40	0.005	0.1

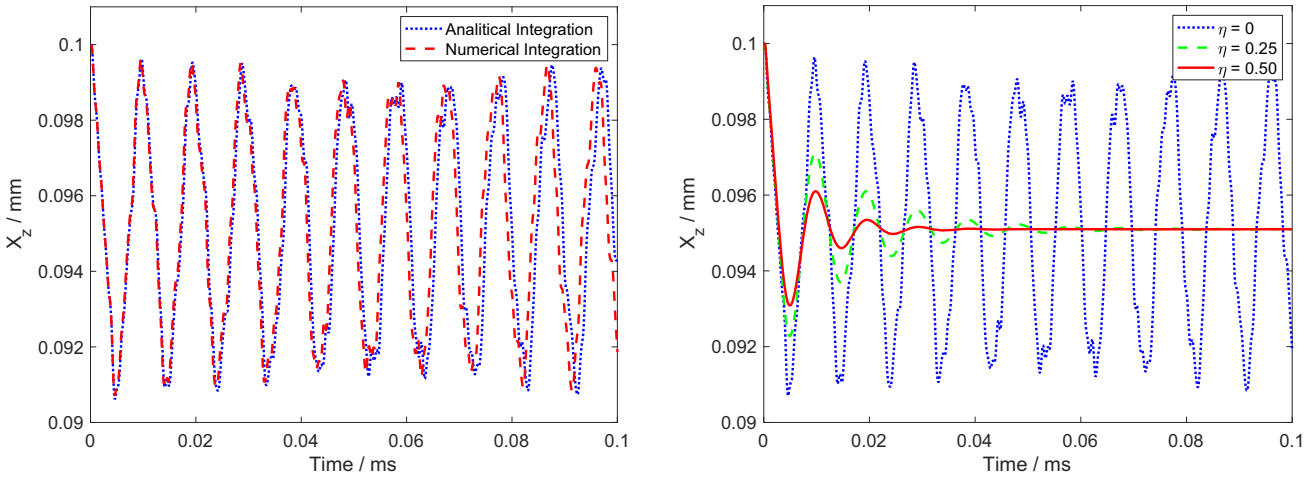

Fig. 4 **a** Validation of the derived strain energy and **b** the damping effect on the top beam node

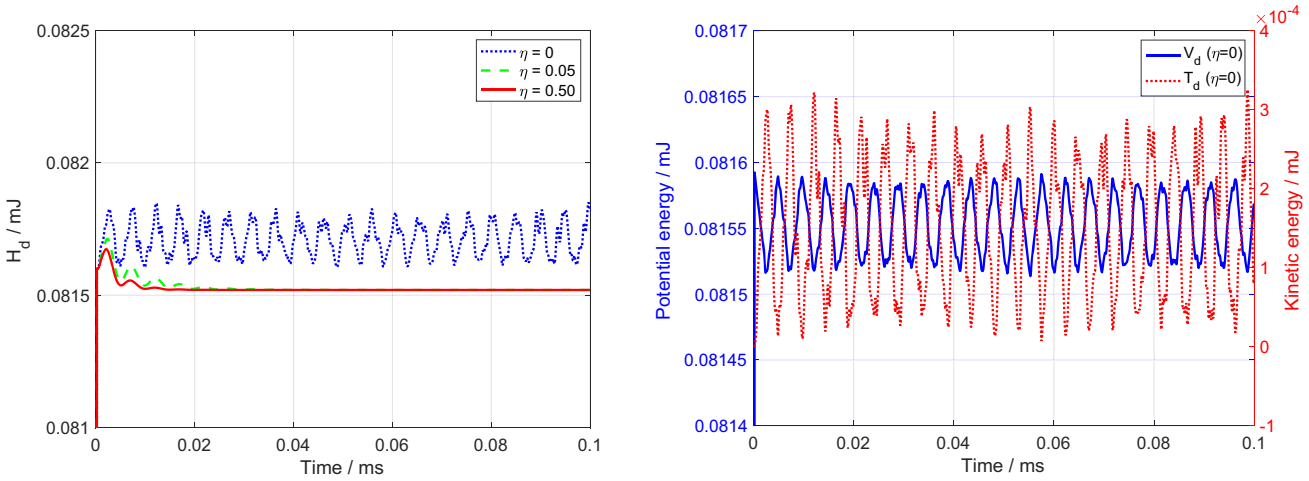

Fig. 5 Energy behavior of the beam

to the 3D FEM model by fixing the horizontal movement of the finite element nodes, leading to a fairer comparison between the 3D FEM model and the beam model.

The magnitude of contractions computed by these two approaches is compared in Fig. 7a. It can be observed that the contractions are converged for both models with the decrease of mesh size. Additionally, the contractions of beam model are very close to the 3D finite element model. The small deviation at $\phi = 8 \times 10^4$ V is induced by the approximation of the logarithm terms in the beam strain energy, see Eq. (90). When the higher order terms of the Taylor series expansion are involved, the deviation will be smaller. In the beam model, 15 degrees of freedom are attached on each node. In the 3D FEM model, 16 degrees of freedom are required at each beam

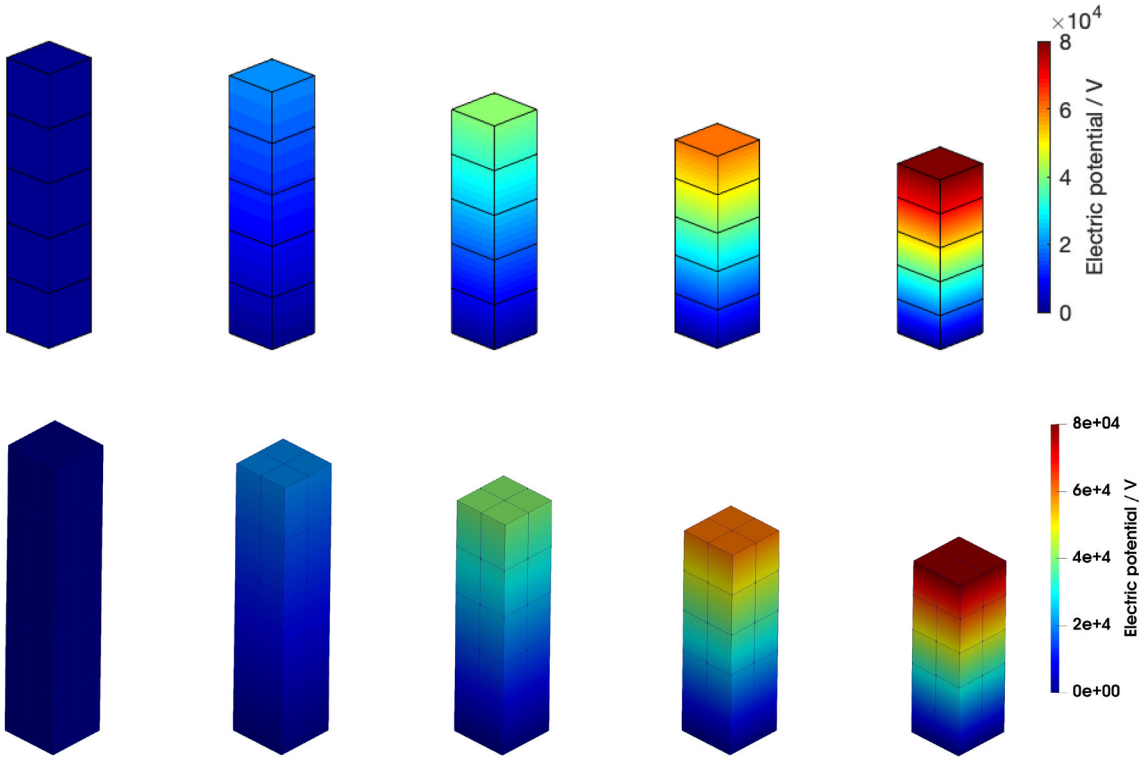

Fig. 6 Contractions in the beam model (upper) and the 3D FEM model (lower) with electric potentials $\phi_o = 0, 2, 4, 6, 8 \times 10^4$ V

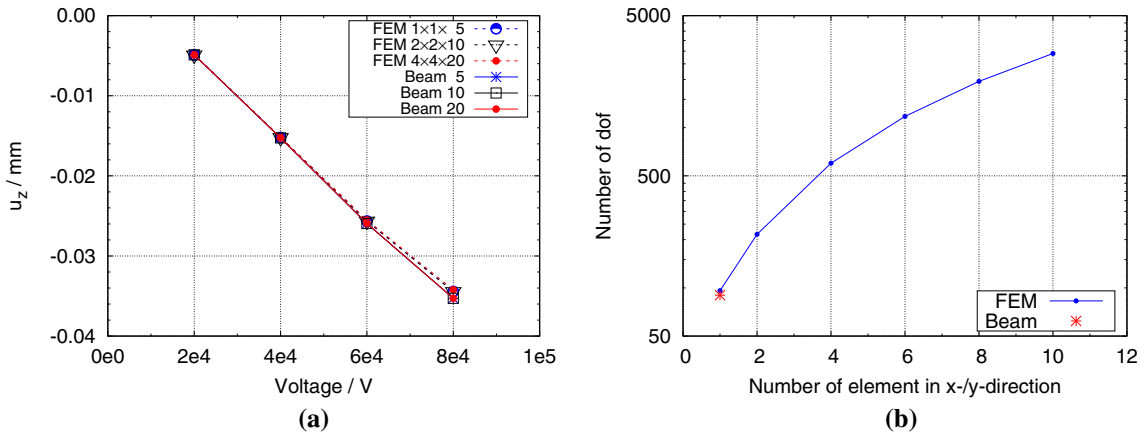

Fig. 7 **a** Displacement of the top beam node and **b** degree of freedom of the beam

cross section when the cross section is discretized with one element. However, the number of degree of freedom in the 3D FEM model increases with the increase of number of elements on the cross section as shown in Fig. 7b. It can be observed that, for the same number of elements (5 elements in Fig. 7b) in the longitudinal direction, less degrees of freedom are required in the beam model.

7.2 Shear

Apart form the uniaxial contraction, the electric potential formulated in this work allows for more complex beam deformations by applying a non-uniform electric potential on the cross sections. To generate shear in the beam, the electric potential $\phi_i = 2 \times 10^2 + i4 \times 10^2 + 2 \times 10^4 X^1$ is applied to electrode i as shown in Table 2. The electric potential on the deformed beam at time $t = 0.5$ ms is shown in Fig. 8a, where the beam is discretized with 60 finite elements (20 DEA cells) and the damping parameter η is set to be 3. By applying

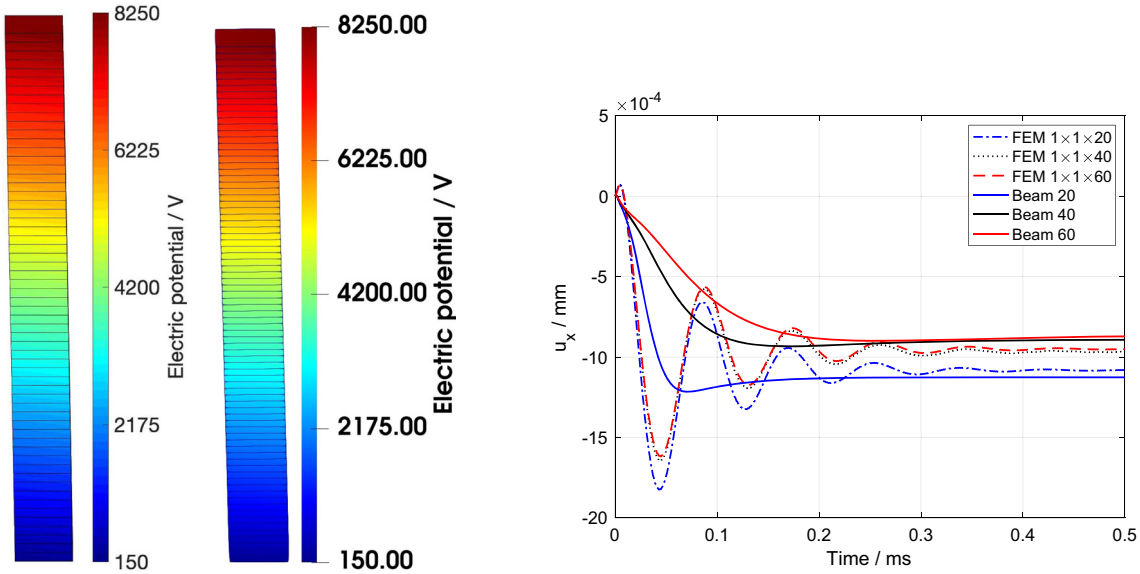

(a) Beam **(b)** 3D FEM **(c)** Displacement of the top beam node

Fig. 8 Shear in the beam model and the 3D FEM model

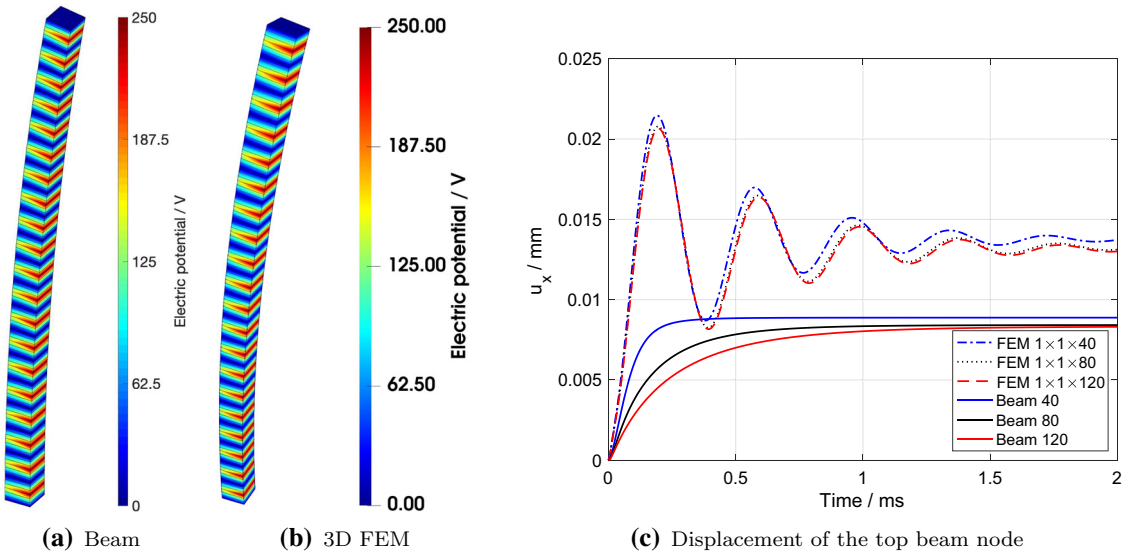

(a) Beam **(b)** 3D FEM **(c)** Displacement of the top beam node

Fig. 9 Bending in the beam model and the 3D FEM model

the same electrical boundary conditions, the deformation is computed by the 3D FEM model as shown in Fig. 8b. The displacement of the top beam node is depicted in Fig. 8c, where the beam is discretized with 20, 40 and 60 elements, respectively. It can be observed that the displacements are converged in the fine mesh and the beam model is close to the 3D FEM model.

7.3 Bending

As shown in Table 2, the bending of the beam can be obtained by alternately applying zero and the non-uniform electric potential $\phi = 2 \times 10^2 + 2 \times 10^4 X^1$ on the cross sections of beam. In this case, the non-uniform contraction of each DEA cell leads to the overall bending of beam. The deformed state of the beam model at time $t = 2$ ms is compared with the 3D FEM model in Fig. 9. According to Fig. 9c, the displacement is converged with the decrease of mesh size for both models. However there is deviation of displacement during the dynamic process as well as at the steady state, which can be attributed to the deformation of the cross section in 3D FEM model. The deformation of cross section makes the beam softer thus the displacement u_x of the 3D FEM model is larger than the beam model.

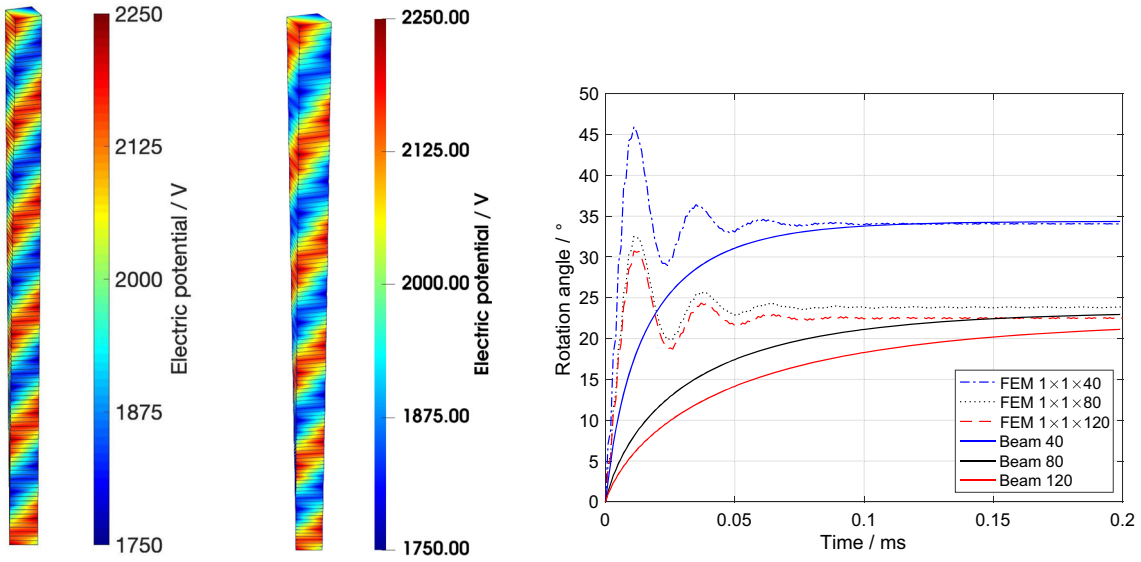

(a) Beam **(b)** 3D FEM **(c)** Rotation angle of the top beam node

Fig. 10 Torsion in the beam model and the 3D FEM model

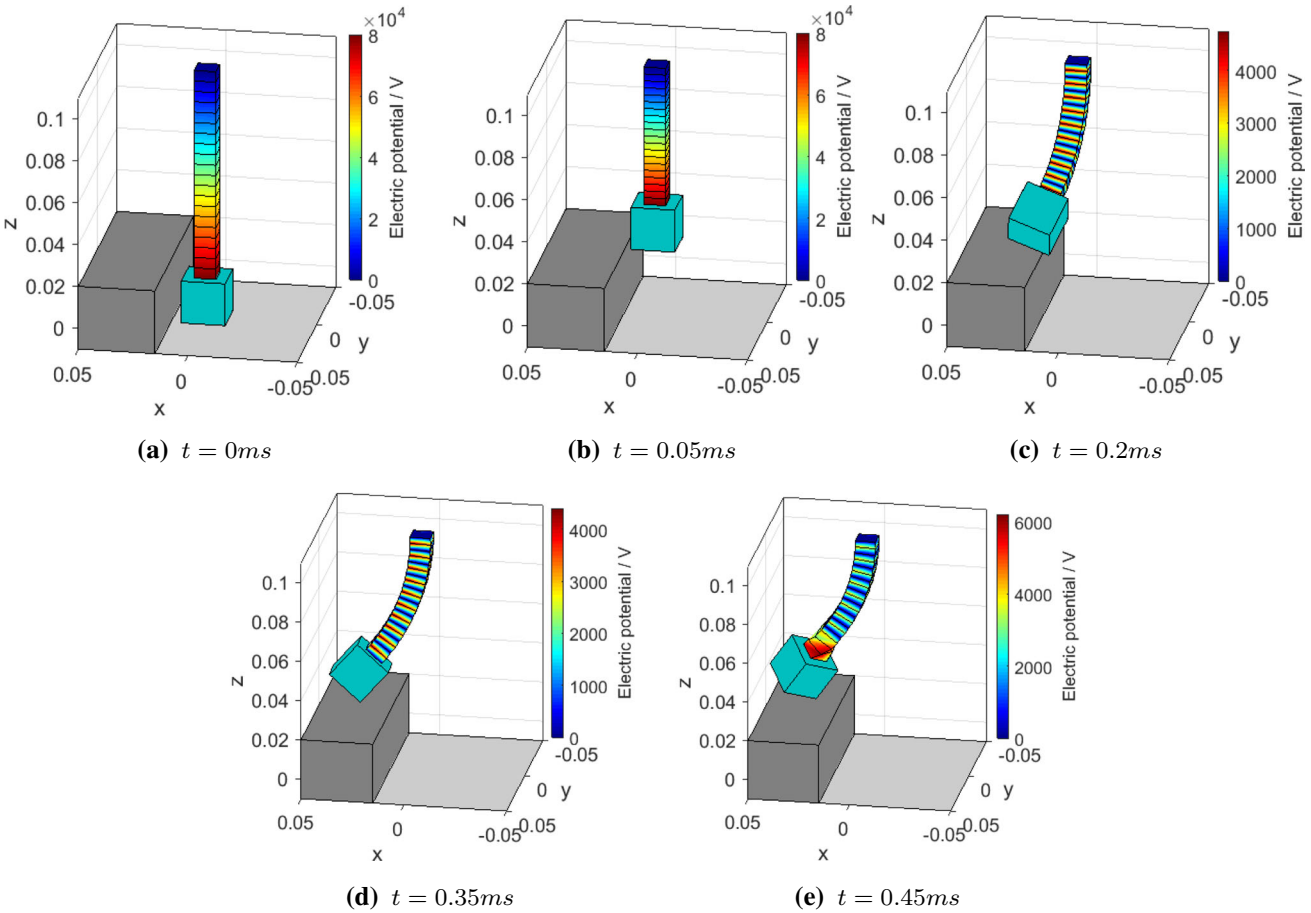

(a) $t = 0ms$ **(b)** $t = 0.05ms$ **(c)** $t = 0.2ms$

(d) $t = 0.35ms$ **(e)** $t = 0.45ms$

Fig. 11 A soft robotic arm moving a package from the ground to a desk

7.4 Torsion

This part is devoted to the torsion of the beam where the torque around the beam axis has to be generated by applying the electric potential. To this end, the spiral distribution of electric potential along beam axis is applied. In this example, the beam is composed of $N_c = 40$ stacked DEA cells. The electric potential ϕ_i in Table 2 is applied to the cross section of the beam node with electrode i attached. The angle θ_i in the electric potential is set to be $\theta_i = i\frac{\pi}{4}$. The torsion of the beam model at time $t = 0.2$ ms is compared with the 3D FEM model in Fig. 10, where the beam is discretized with 120 elements in the longitudinal direction in both models.

The rotation angle of the top beam node is shown in Fig. 10c, where the beam is discretized with 40, 80 and 120 elements in the longitudinal direction, respectively. It can be observed that the rotation angles computed with the beam model and the 3D FEM model are very close at time $t = 0.2$ ms. With the finer mesh, the rotation angles are approaching to the converged value. Additionally, the large deviation can be observed at the beginning of the loading, which is induced by the deformation of the cross section in the 3D FEM model during the rotation.

7.5 Robotic arm

As an example of the combination of different deformation modes, the beam model is applied in this part to simulate a simplified robotic arm holding a package as shown in Fig. 11. The package is represented by an additional point mass concentrated at the beam's free end. The beam has the length $l = 0.1$ mm and a square cross section with width $b = 0.01$ mm. The mass of package is set to be 2 times the mass of beam. The beam is composed with 20 DEA cells and discretized with 20 finite elements.

As shown in Fig. 11a, b , the package is fist lifted from ground by the uniaxial contraction of the beam, where the constant electric potentials $\phi_1 = 8 \times 10^4$ V and $\phi_{21} = 0$ V are applied to the beam's fixed and free end, respectively, until $t = 0.05$ ms. Then, from $t = 0.051$ to $t = 0.2$ ms, the bending of the beam is generated by changing the electric boundary conditions to $\phi_i = 4 \times 10^3 + 8 \times 10^4(cos\frac{\pi}{8} - sin\frac{\pi}{8})X^1 + 8 \times 10^4(cos\frac{\pi}{8} + sin\frac{\pi}{8})X^2\, V$, $(i = 2, 4, ...)$ and $\phi_i = 0V(i = 1, 3, ...)$, which leads to the moving of the package to the desk, as shown in Fig. 11c. From $t = 0.201$ to $t = 0.35$ ms, the bending of the beam in another direction is generated by changing the electric boundary conditions to $\phi_i = 4 \times 10^3 + 8 \times 10^4 X^1\, V$, $(i = 2, 4, ...)$, as shown in Fig. 11d. To rotate the package on the desk as shown in Fig. 11e, the electric boundary conditions $\phi_i = 4 \times 10^3 + 2 \times 10^5(cos\theta_i - sin\theta_i)X^1 + 2 \times 10^5(cos\theta_i + sin\theta_i)X^2\, V$ are imposed on the last three beam nodes from $t = 0.351$ to $t = 0.45$ ms. In the simulation, the damping effect is imposed by setting $\eta = 0.6$ in the viscoelastic model such that the beam is gradually approaching a steady state.

8 Conclusion

In this paper, an electromechanically coupled viscoelastic beam model is developed. Based on the governing equations, the kinematics as well as the strain energy functions in continuum electromechanics, their counterparts in Cosserat beam are formulated consistently. Especially, the proposed formulation of the electric potential allows for all types of the dielectric induced deformations in the beam, such as contraction, shear, bending and torsion. In the uniaxial contractions of the beam, the oscillation of the beam is induced by the contractive electric forces, where the damping effect in the motion of the beam node is observed after introducing the viscoelastic effect. Additionally, the damping behavior of the total energy is observed as well, where the discrete Hamiltonian is evaluated. Another interesting point is that the oscillation frequency of the potential energy in the dielectric elastomer is twice as much as that of the displacement, which can be attributed to the fact that the potential energy is in its maximum value in the undeformed state of the charged dielectric elastomer. The simulation results show that the beam model agrees well with the 3D FEM model in contraction, shear, bending and torsion, however less degrees of freedom are required in the beam model. It can be also observed that the beam DEAs have large flexibility of motion by combining different deformation modes.

Acknowledgements The authors acknowledge the support of Deutsche Forschungsgemeinschaft (DFG) with the project: LE 1841-/5-11.

Funding Open Access funding enabled and organized by Projekt DEAL.

Appendix

The aim of this appendix is to derive the strain energy function Ω_b for beam in Eq. (62). The strain energy function $\Omega(\mathbf{C}, J, \mathbf{E}^e)$ in Eq. (60) can be rewritten in terms of beam

strain measures $\boldsymbol{\Gamma}, \mathbf{K}, \boldsymbol{\gamma}, \boldsymbol{\kappa}, \boldsymbol{\varepsilon}, \mathbf{e}$

$$
\begin{aligned}
&\Omega(\boldsymbol{\Gamma}, \mathbf{K}, \boldsymbol{\gamma}, \boldsymbol{\kappa}, \boldsymbol{\varepsilon}, \mathbf{e}, \mathbf{X}) \\
&\quad = \Omega(\mathbf{C}, J, \mathbf{E}^e) \\
&\quad = \underbrace{\frac{\mu}{2}\left[2(\mathbf{a}^r \cdot \mathbf{d}_3^0) + \mathbf{a}^r \cdot \mathbf{a}^r\right] - \mu \ln(1 + \mathbf{a} \cdot \mathbf{d}_3^t) + \frac{\lambda}{2}\left[\ln(1 + \mathbf{a} \cdot \mathbf{d}_3^t)\right]^2}_{\Omega_1} \\
&\qquad + c_1\left[\varepsilon_1^2 + \varepsilon_2^2 + (\varepsilon_3 + \mathbf{e} \cdot \mathbf{X})^2\right] \\
&\qquad + c_2\left[\varepsilon_1^2 + \varepsilon_2^2 + (1 + \mathbf{a}^r \cdot \mathbf{a}^r)(\varepsilon_3 + \mathbf{e} \cdot \mathbf{X})^2\right] \\
&\qquad + \underbrace{c_2\left\{2(\varepsilon_3 + \mathbf{e} \cdot \mathbf{X})\left[\varepsilon_1(\mathbf{d}_1^0 \cdot \mathbf{a}^r) + \varepsilon_2(\mathbf{d}_2^0 \cdot \mathbf{a}^r) + (\varepsilon_3 + \mathbf{e} \cdot \mathbf{X})(\mathbf{d}_3^0 \cdot \mathbf{a}^r)\right]\right\}}_{\Omega_2},
\end{aligned}
\tag{88}
$$

where $\mathbf{d}_i^0$ denotes $\mathbf{d}_i(s, 0)$, $\mathbf{d}_i^t$ denotes $\mathbf{d}_i(s, t)$, ε_i are the components of the strain-like vector $\boldsymbol{\varepsilon}$ in Eq. (52), $\mathbf{X}$ is the vector $\mathbf{X} = \begin{bmatrix} X^1 & X^2 & 0 \end{bmatrix}$ and $\mathbf{e}$ is the electrical variable defined as $\mathbf{e}(s) = \begin{bmatrix} \frac{\partial \alpha^s}{\partial s} & \frac{\partial \beta^s}{\partial s} & 0 \end{bmatrix}^T$.

The strain energy function for the beam is obtained by integrating $\Omega(\boldsymbol{\Gamma}, \mathbf{K}, \boldsymbol{\gamma}, \boldsymbol{\kappa}, \boldsymbol{\varepsilon}, \mathbf{e}, \mathbf{X})$ over the cross section

$$
\begin{aligned}
&\Omega_b(\boldsymbol{\Gamma}, \mathbf{K}, \boldsymbol{\gamma}, \boldsymbol{\kappa}, \boldsymbol{\varepsilon}, \mathbf{e}) \\
&\quad = \int_\Sigma \Omega(\boldsymbol{\Gamma}, \mathbf{K}, \boldsymbol{\gamma}, \boldsymbol{\kappa}, \boldsymbol{\varepsilon}, \mathbf{e}, \mathbf{X}) dA = \Omega_{b1} + \Omega_{b2}
\end{aligned}
\tag{89}
$$

with

$$
\begin{aligned}
\Omega_{b1} &= \int_\Sigma \Omega_1 dA \\
&= \int_\Sigma \left\{ \frac{\mu}{2}\left[2(\mathbf{a}^r \cdot \mathbf{d}_3^0) + \mathbf{a}^r \cdot \mathbf{a}^r\right] \right. \\
&\quad \left. - \mu \ln(1 + \mathbf{a} \cdot \mathbf{d}_3^t) + \frac{\lambda}{2}\left[\ln(1 + \mathbf{a} \cdot \mathbf{d}_3^t)\right]^2 \right\} dA \\
&\approx \int_\Sigma \left\{ \frac{\mu}{2}\left[2(\mathbf{a}^r \cdot \mathbf{d}_3^0) + \mathbf{a}^r \cdot \mathbf{a}^r\right) \right. \\
&\quad \left. - \mu\left[\mathbf{a} \cdot \mathbf{d}_3^t - \frac{(\mathbf{a} \cdot \mathbf{d}_3^t)^2}{2}\right] + \frac{\lambda}{2}\left[\mathbf{a} \cdot \mathbf{d}_3^t - \frac{(\mathbf{a} \cdot \mathbf{d}_3^t)^2}{2}\right]^2 \right\} dA \\
&= C_1 J_{1111} + C_2 J_{1122} + C_3 J_{11} + C_4 J_{2222} + C_5 J_{22} + C_6
\end{aligned}
\tag{90}
$$

and

$$
\begin{aligned}
\Omega_{b2} &= \int_\Sigma \Omega_2 dA \\
&= \int_\Sigma c_1\left[\varepsilon_1^2 + \varepsilon_2^2 + (\varepsilon_3 + \mathbf{e} \cdot \mathbf{X})^2\right] dA \\
&\quad + c_2 \int_\Sigma \left[\varepsilon_1^2 + \varepsilon_2^2 + (1 + \mathbf{a}^r \cdot \mathbf{a}^r)(\varepsilon_3 + \mathbf{e} \cdot \mathbf{X})^2\right] + \\
&\quad 2(\varepsilon_3 + \mathbf{e} \cdot \mathbf{X})\left[\varepsilon_1(\mathbf{d}_1^0 \cdot \mathbf{a}^r) + \varepsilon_2(\mathbf{d}_2^0 \cdot \mathbf{a}^r)\right. \\
&\quad \left. + (\varepsilon_3 + \mathbf{e} \cdot \mathbf{X})(\mathbf{d}_3^0 \cdot \mathbf{a}^r)\right] dA \\
&= C_7 J_{1111} + C_8 J_{1122} + C_9 J_{11} \\
&\quad + C_{10} J_{2222} + C_{11} J_{22} + C_{12},
\end{aligned}
\tag{91}
$$

where the area moments are given by $J_{1111} = \int_\Sigma X_1^4 dA$, $J_{2222} = \int_\Sigma X_2^4 dA$, $J_{1122} = \int_\Sigma X_1^2 X_2^2 dA$, $J_{11} = \int_\Sigma X_1^2 dA$, $J_{22} = \int_\Sigma X_2^2 dA$, other area moments are zero due to the symmetry of the cross section in this work.

The coefficients in Ω_{b1} and Ω_{b2} are given by

$$
\begin{aligned}
C_1 &= \frac{\lambda}{8}\left[d_{31}(d_{21}\kappa_3 + d_{31}\kappa_2) + d_{32}(d_{22}\kappa_3 + d_{32}\kappa_2)\right. \\
&\quad \left. + d_{33}(d_{23}\kappa_3 + d_{33}\kappa_2)\right]^4,
\end{aligned}
\tag{92}
$$

$$
\begin{aligned}
C_2 &= \frac{3}{4}\lambda\left[d_{31}(d_{11}\kappa_3 - d_{31}\kappa_1) + d_{32}(d_{12}\kappa_3 - d_{32}\kappa_1)\right. \\
&\quad \left. + d_{33}(d_{13}\kappa_3 - d_{33}\kappa_1)\right]^2 \\
&\quad \cdot \left[d_{31}(d_{21}\kappa_3 + d_{31}\kappa_2) + d_{32}(d_{22}\kappa_3 + d_{32}\kappa_2)\right. \\
&\quad \left. + d_{33}(d_{23}\kappa_3 + d_{33}\kappa_2)\right]^2,
\end{aligned}
\tag{93}
$$

$$
\begin{aligned}
C_3 &= \frac{\mu}{2}\left[(d_{21}^0 K_3 + d_{31}^0 K_2)^2 + (d_{22}^0 K_3 + d_{32}^0 K_2)^2\right. \\
&\quad \left. + (d_{23}^0 K_3 + d_{33}^0 K_2)^2\right] \\
&\quad + \frac{\mu}{2}\left[d_{31}(d_{21}\kappa_3 + d_{31}\kappa_2) + d_{32}(d_{22}\kappa_3 + d_{32}\kappa_2)\right. \\
&\quad \left. + d_{33}(d_{23}\kappa_3 + d_{33}\kappa_2)\right]^2 \\
&\quad - \frac{\lambda}{2}\left[d_{31}(d_{21}\kappa_3 + d_{31}\kappa_2) + d_{32}(d_{22}\kappa_3 + d_{32}\kappa_2)\right. \\
&\quad \left. + d_{33}(d_{23}\kappa_3 + d_{33}\kappa_2)\right]^2 \\
&\quad \cdot \left[d_{31}\gamma_1 + d_{32}\gamma_2 + d_{33}\gamma_3\right. \\
&\quad \left. - \frac{(d_{31}\gamma_1 + d_{32}\gamma_2 + d_{33}\gamma_3)^2}{2}\right] \\
&\quad + \frac{\lambda}{2}\left\{d_{31}(d_{21}\kappa_3 + d_{31}\kappa_2)\right. \\
&\quad - \left[d_{31}(d_{21}\kappa_3 + d_{31}\kappa_2) + d_{32}(d_{22}\kappa_3 + d_{32}\kappa_2)\right. \\
&\quad \left. + d_{33}(d_{23}\kappa_3 + d_{33}\kappa_2)\right](d_{31}\gamma_1 + d_{32}\gamma_2 + d_{33}\gamma_3) \\
&\quad \left. + d_{32}(d_{22}\kappa_3 + d_{32}\kappa_2) + d_{33}(d_{23}\kappa_3 + d_{33}\kappa_2)\right\}^2,
\end{aligned}
\tag{94}
$$

$$
\begin{aligned}
C_4 &= \frac{\lambda}{8}\left[d_{31}(d_{11}\kappa_3 - d_{31}\kappa_1) + d_{32}(d_{12}\kappa_3 - d_{32}\kappa_1)\right. \\
&\quad \left. + d_{33}(d_{13}\kappa_3 - d_{33}\kappa_1)\right]^4,
\end{aligned}
\tag{95}
$$

$$
\begin{aligned}
C_5 &= \frac{\mu}{2}\left[(d_{11}^0 K_3 - d_{31}^0 K_1)^2 + (d_{12}^0 K_3 - d_{32}^0 K_1)^2\right. \\
&\quad \left. + (d_{13}^0 K_3 - d_{33}^0 K_1)^2\right] \\
&\quad + \frac{\mu}{2}\left[d_{31}(d_{11}\kappa_3 - d_{31}\kappa_1) + d_{32}(d_{12}\kappa_3 - d_{32}\kappa_1)\right. \\
&\quad \left. + d_{33}(d_{13}\kappa_3 - d_{33}\kappa_1)\right]^2 \\
&\quad - \frac{\lambda}{2}\left[d_{31}(d_{11}\kappa_3 - d_{31}\kappa_1) + d_{32}(d_{12}\kappa_3 - d_{32}\kappa_1)\right. \\
&\quad \left. + d_{33}(d_{13}\kappa_3 - d_{33}\kappa_1)\right]^2 \\
&\quad \cdot \left[d_{31}\gamma_1 + d_{32}\gamma_2 + d_{33}\gamma_3\right. \\
&\quad \left. - \frac{(d_{31}\gamma_1 + d_{32}\gamma_2 + d_{33}\gamma_3)^2}{2}\right]
\end{aligned}
$$

$$
\begin{aligned}
&+\frac{\lambda}{2}\{d_{31}(d_{11}\kappa_3-d_{31}\kappa_1)-[d_{31}(d_{11}\kappa_3-d_{31}\kappa_1)\\
&+d_{32}(d_{12}\kappa_3-d_{32}\kappa_1)\\
&+d_{33}(d_{13}\kappa_3-d_{33}\kappa_1)]\\
&\cdot(d_{31}\gamma_1+d_{32}\gamma_2+d_{33}\gamma_3)+d_{32}(d_{12}\kappa_3-d_{32}\kappa_1)\\
&+d_{33}(d_{13}\kappa_3-d_{33}\kappa_1)\}^2, \qquad (96)
\end{aligned}
$$

$$
\begin{aligned}
C_6=&\frac{\mu}{2}(\Gamma_1^2+2d_{31}^0\Gamma_1+\Gamma_2^2\\
&+2d_{32}^0\Gamma_2+\Gamma_3^2+2d_{33}^0\Gamma_3)\\
&+\mu\left[d_{31}\gamma_1+d_{32}\gamma_2+d_{33}\gamma_3\right.\\
&\left.-\frac{(d_{31}\gamma_1+d_{32}\gamma_2+d_{33}\gamma_3)^2}{2}\right]\\
&+\frac{\lambda}{2}\left[d_{31}\gamma_1+d_{32}\gamma_2+d_{33}\gamma_3\right.\\
&\left.-\frac{(d_{31}\gamma_1+d_{32}\gamma_2+d_{33}\gamma_3)^2}{2}\right]^2, \qquad (97)\\
C_7=&c_2e_1^2\left[(d_{21}^0K_3+d_{31}^0K_2)^2+(d_{22}^0K_3+d_{32}^0K_2)^2\right.\\
&\left.+(d_{23}^0K_3+d_{33}^0K_2)^2\right], \qquad (98)\\
C_8=&c_2\left\{e_1^2\left[(d_{11}^0K_3-d_{31}^0K_1)^2+(d_{12}^0K_3-d_{32}^0K_1)^2\right.\right.\\
&\left.+(d_{13}^0K_3-d_{33}^0K_1)^2\right]\\
&+e_2^2\left[(d_{21}^0K_3+d_{31}^0K_2)^2+(d_{22}^0K_3+d_{32}^0K_2)^2\right.\\
&\left.+(d_{23}^0K_3+d_{33}^0K_2)^2\right]\\
&-2e_1e_2\left[2(d_{11}^0K_3-d_{31}^0K_1)(d_{21}^0K_3+d_{31}^0K_2)\right.\\
&\left.+2(d_{12}^0K_3-d_{32}^0K_1)(d_{22}^0K_3+d_{32}^0K_2)\right]\\
&\left.-2e_1e_2\left[2(d_{13}^0K_3-d_{33}^0K_1)(d_{23}^0K_3+d_{33}^0K_2)\right]\right\}, \qquad (99)\\
C_9=&c_2\varepsilon_3^2\left[(d_{21}^0K_3+d_{31}^0K_2)^2+(d_{22}^0K_3+d_{32}^0K_2)^2\right.\\
&\left.+(d_{23}^0K_3+d_{33}^0K_2)^2\right]\\
&+c_2e_1^2(\Gamma_1^2+\Gamma_2^2+\Gamma_3^2+1)\\
&+2c_2e_1\varepsilon_1\left[d_{11}^0(d_{21}^0K_3+d_{31}^0K_2)+d_{12}^0(d_{22}^0K_3+d_{32}^0K_2)\right.\\
&\left.+d_{13}^0(d_{23}^0K_3+d_{33}^0K_2)\right]\\
&+2c_2e_1\varepsilon_2\left[d_{21}^0(d_{21}^0K_3+d_{31}^0K_2)+d_{22}^0(d_{22}^0K_3+d_{32}^0K_2)\right.\\
&\left.+d_{23}^0(d_{23}^0K_3+d_{33}^0K_2)\right]\\
&+2c_2e_1\varepsilon_3\left[d_{31}^0(d_{21}^0K_3+d_{31}^0K_2)+d_{32}^0(d_{22}^0K_3\right.\\
&\left.+d_{32}^0K_2)+d_{33}^0(d_{23}^0K_3+d_{33}^0K_2)\right]\\
&+2c_2e_1e_1(d_{31}^0\Gamma_1+d_{32}^0\Gamma_2+d_{33}^0\Gamma_3)\\
&+2c_2\varepsilon_3e_1(d_{31}^0(d_{21}^0K_3+d_{31}^0K_2)+d_{32}^0(d_{22}^0K_3+d_{32}^0K_2)\\
&+d_{33}^0(d_{23}^0K_3+d_{33}^0K_2))\\
&+2c_2\varepsilon_3e_1(2\Gamma_1(d_{21}^0K_3+d_{31}^0K_2)+2\Gamma_2(d_{22}^0K_3+d_{32}^0K_2)\\
&+2\Gamma_3(d_{23}^0K_3+d_{33}^0K_2))\\
&+c_1e_1^2, \qquad (100)\\
C_{10}=&c_2e_2^2\left[(d_{11}^0K_3-d_{31}^0K_1)^2+(d_{12}^0K_3-d_{32}^0K_1)^2\right.\\
&\left.+(d_{13}^0K_3-d_{33}^0K_1)^2\right], \qquad (101)\\
C_{11}=&c_1e_2^2\\
&-2c_2e_2\varepsilon_1\left[d_{11}^0(d_{11}^0K_3-d_{31}^0K_1)+d_{12}^0(d_{12}^0K_3-d_{32}^0K_1)\right.\\
&\left.+d_{13}^0(d_{13}^0K_3-d_{33}^0K_1)\right]\\
&-2c_2e_2\varepsilon_2\left[d_{21}^0(d_{11}^0K_3-d_{31}^0K_1)+d_{22}^0(d_{12}^0K_3-d_{32}^0K_1)\right.\\
&\left.+d_{23}^0(d_{13}^0K_3-d_{33}^0K_1)\right]\\
&-2c_2e_2\varepsilon_3\left[d_{31}^0(d_{11}^0K_3-d_{31}^0K_1)+d_{32}^0(d_{12}^0K_3-d_{32}^0K_1)\right.\\
&\left.+d_{33}^0(d_{13}^0K_3-d_{33}^0K_1)\right]\\
&+2c_2e_2e_2(d_{31}^0\Gamma_1+d_{32}^0\Gamma_2+d_{33}^0\Gamma_3)\\
&+c_2e_2^2(\Gamma_1^2+\Gamma_2^2+\Gamma_3^2+1)\\
&+c_2\varepsilon_3^2\left[(d_{11}^0K_3-d_{31}^0K_1)^2+(d_{12}^0K_3-d_{32}^0K_1)^2\right.\\
&\left.+(d_{13}^0K_3-d_{33}^0K_1)^2\right]\\
&-2c_2\varepsilon_3e_2\left[d_{31}^0(d_{11}^0K_3-d_{31}^0K_1)+d_{32}^0(d_{12}^0K_3-d_{32}^0K_1)\right.\\
&\left.+d_{33}^0(d_{13}^0K_3-d_{33}^0K_1)\right]\\
&-2c_2\varepsilon_3e_2\left[2\Gamma_1(d_{11}^0K_3-d_{31}^0K_1)+2\Gamma_2(d_{12}^0K_3-d_{32}^0K_1)\right.\\
&\left.+2\Gamma_3(d_{13}^0K_3-d_{33}^0K_1)\right], \qquad (102)\\
C_{12}=&c_1(\varepsilon_1^2+\varepsilon_2^2+\varepsilon_3^2)\\
&+2c_2\varepsilon_3\left[\varepsilon_1(d_{11}^0\Gamma_1+d_{12}^0\Gamma_2+d_{13}^0\Gamma_3)\right.\\
&+\varepsilon_2(d_{21}^0\Gamma_1+d_{22}^0\Gamma_2+d_{23}^0\Gamma_3)\\
&\left.+\varepsilon_3(d_{31}^0\Gamma_1+d_{32}^0\Gamma_2+d_{33}^0\Gamma_3)\right]\\
&+c_2\left[\varepsilon_1^2+\varepsilon_2^2+\varepsilon_3^2(\Gamma_1^2+\Gamma_2^2+\Gamma_3^2+1)\right]. \qquad (103)
\end{aligned}
$$

In the above formulations, $(\cdot)_i (i = 1, 2, 3)$ denote the components of the vector $(\cdot)$, such as e_1 is the first component of the vector $\mathbf{e}$ and d_{12}^0 is the second component of the vector $\mathbf{d}_1(s, 0)$.

References

1. Andersson JAE, Gillis J, Horn G, Rawlings JB, Diehl M (2019) CasADi—a software framework for nonlinear optimization and optimal control. Math Program Comput 11(1):1–36
2. Antman SS (2005) Nonlinear problems of elasticity. Springer, Berlin

3. Armero F, Romero I (2001) On the formulation of high-frequency dissipative time-stepping algorithms for nonlinear dynamics. Part i: low-order methods for two model problems and nonlinear elastodynamics. Comput Methods Appl Mech Eng 190(20):2603–2649
4. Auricchio F, Carotenuto P, Reali A (2008) On the geometrically exact beam model: a consistent, effective and simple derivation from three-dimensional finite-elasticity. Int J Solids Struct 45(17):4766–4781
5. Bar-Cohen Y (2000) Electroactive polymers as artificial muscles: capabilities, potentials and challenges. Robotics 2000:188–196
6. Betsch P, Leyendecker S (2006) The discrete null space method for the energy consistent integration of constrained mechanical systems. Part ii: multibody dynamics. Int J Numer Methods Eng 67(4):499–552
7. Cosserat E, Cosserat F (1909) Théorie des corps déformables. A. Hermann et fils, Paris
8. Dorfmann A, Ogden RW (2005) Nonlinear electroelasticity. Acta Mech 174(3–4):167–183
9. Duduta M, Hajiesmaili E, Zhao H, Wood RJ, Clarke DR (2019) Realizing the potential of dielectric elastomer artificial muscles. Proc Natl Acad Sci 116(7):2476–2481
10. Eugster SR, Hesch C, Betsch P, Glocker Ch (2014) Director-based beam finite elements relying on the geometrically exact beam theory formulated in skew coordinates. Int J Numer Methods Eng 97(2):111–129
11. Feng C, Jiang L, Lau WM (2011) Dynamic characteristics of a dielectric elastomer-based microbeam resonator with small vibration amplitude. J Micromech Microeng 21(9):095002
12. Greaney P, Meere M, Zurlo G (2019) The out-of-plane behaviour of dielectric membranes: description of wrinkling and pull-in instabilities. J Mech Phys Solids 122:84–97
13. Khan KA, Wafai H, El Sayed T (2013) A variational constitutive framework for the nonlinear viscoelastic response of a dielectric elastomer. Comput Mech 52(2):345–360
14. Kovacs G, Düring L, Michel S, Terrasi G (2009) Stacked dielectric elastomer actuator for tensile force transmission. Sens Actuators A 155(2):299–307
15. Krommer M, Irschik H (2002) An electromechanically coupled theory for piezoelastic beams taking into account the charge equation of electrostatics. Acta Mech 154(1–4):141–158
16. Leyendecker S, Marsden JE, Ortiz M (2008) Variational integrators for constrained dynamical systems. ZAMM J Appl Math Mech 88(9):677–708
17. Löwe C, Zhang X, Kovacs G (2005) Dielectric elastomers in actuator technology. Adv Eng Mater 7(5):361–367
18. Marsden JE, Ratiu TS (2013) Introduction to mechanics and symmetry: a basic exposition of classical mechanical systems, vol 17. Springer, Berlin
19. Ortigosa R, Franke M, Janz A, Gil AJ, Betsch P (2018) An energy–momentum time integration scheme based on a convex multi-variable framework for non-linear electro-elastodynamics. Comput Methods Appl Mech Eng 339:1–35
20. Pao YH (1978) Electromagnetic forces in deformable continua. In: Nemat-Nasser S (ed) Mechanics today (A78-35706 14-70). Pergamon New York, vol 4, pp 209–305
21. Pelrine RE, Kornbluh RD, Joseph JP (1998) Electrostriction of polymer dielectrics with compliant electrodes as a means of actuation. Sens Actuators A 64(1):77–85
22. Romero Ignacio, Armero F (2002) An objective finite element approximation of the kinematics of geometrically exact rods and its use in the formulation of an energy–momentum conserving scheme in dynamics. Int J Numer Methods Eng 54(12):1683–1716
23. Schlögl T, Leyendecker S (2016a) Dynamic simulation of dielectric elastomer actuated multibody systems. In: Jovanova J, Anachkova M, Gavriloski V, Petrevski D, Grazhdani F, Pecioski D (eds) Multifunctional materials; Mechanics and behavior of active materials; Integrated system design and implementation. Smart materials, adaptive structures and intelligent systems, vol 1. American Society of Mechanical Engineers, New york. https://doi.org/10.1115/SMASIS2016-9110
24. Schlögl T, Leyendecker S (2016) Electrostatic–viscoelastic finite element model of dielectric actuators. Comput Methods Appl Mech Eng 299:421–439
25. Schlögl T, Leyendecker S (2017) A polarisation based approach to model the strain dependent permittivity of dielectric elastomers. Sens Actuators A 267:156–163
26. Schoeftner S, Buchberger G (2012) An electromechanically-coupled Bernoulli–Euler beam theory taking into account the finite conductivity of the electrodes for sensing and actuation. ACEM 12:1051–1065
27. Simo JC (1985) Finite strain beam theory. Comput Methods Appl Mech Eng 49:55–70
28. Simo JC, Vu-Quoc L (1986) A three-dimensional finite-strain rod model. Part ii: computational aspects. Comput Methods Appl Mech Eng 58(1):79–116
29. Simo JC, Vu-Quoc L (1991) A geometrically-exact rod model incorporating shear and torsion-warping deformation. Int J Solids Struct 27(3):371–393
30. Suo Z (2010) Theory of dielectric elastomers. Acta Mech Solida Sin 23(6):549–578
31. Suo Z, Zhao X, Greene WH (2008) A nonlinear field theory of deformable dielectrics. J Mech Phys Solids 56(2):467–486
32. Tadmor EB, Kósa G (2003) Electromechanical coupling correction for piezoelectric layered beams. J Microelectromech Syst 12(6):899–906
33. Vu DK, Steinmann P, Possart G (2007) Numerical modelling of non-linear electroelasticity. Int J Numer Methods Eng 70(6):685–704
34. Wissler M, Mazza E (2007) Electromechanical coupling in dielectric elastomer actuators. Sens Actuators A 138(2):384–393
35. Wriggers P (2008) Nonlinear finite element methods. Springer, Berlin
36. Zhao X, Hong Z, Suo Wand (2007) Electromechanical hysteresis and coexistent states in dielectric elastomers. Phys Rev B 76(13):134113